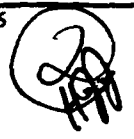


AD-A267 384

TAT N PAGE

Form Approved
OMB No. 0704-0188

1. Average 1 hour per response, including the time for reviewing instructions, searching existing data sources, gathering the collection of information. Send comments regarding this burden estimate or any other aspect of this collection of information, including suggestions for reducing the burden, to Washington Headquarters Services, Directorate for Information Operations and Reports, 1215 Jefferson Davis Highway, Suite 1204, Arlington, VA 22202-4302, and to the Office of Management and Budget, Paperwork Reduction Project (0704-0188), Washington, DC 20503.

1. AGENCY USE ONLY (Leave blank)		2. REPORT DATE		3. REPORT TYPE AND DATES COVERED FINAL/01 DEC 90 TO 31 MAY 93	
4. TITLE AND SUBTITLE TO EXTEND THE THIRTEEN-MOMENT THEORY AND ITS APPLICATION TO PROBLEMS IN RAREFIED HYPERSONIC FLOW				5. FUNDING NUMBERS  2304/A3 61102F AFOSR-91-0104	
6. AUTHOR(S) PROFESSOR H. K. CHENG				8. PERFORMING ORGANIZATION REPORT NUMBER AFOSR-TR- 93 0477	
7. PERFORMING ORGANIZATION NAME(S) AND ADDRESS(ES) UNIVERSITY OF SOUTHERN CALIFORNIA DEPARTMENT OF AEROSPACE ENGINEERING LOS ANGELES, CA 90089				10. SPONSORING / MONITORING AGENCY REPORT NUMBER AFOSR-91-0104	
9. SPONSORING / MONITORING AGENCY NAME(S) AND ADDRESS(ES) AFOSR/NM 110 DUNCAN AVE, SUTE B115 BOLLING AFB DC 20332-0001				10. SPONSORING / MONITORING AGENCY REPORT NUMBER AFOSR-91-0104	
11. SUPPLEMENTARY NOTES					
12a. DISTRIBUTION / AVAILABILITY STATEMENT APPROVED FOR PUBLIC RELEASE: DISTRIBUTION IS UNLIMITED				12b. DISTRIBUTION CODE	
13. ABSTRACT (Maximum 200 words) The theoretical development and supporting particle-simulation (DSMC) and other computational studies carried out during the past two years have strengthened the principle for correlating a flow far from translational equilibrium with the Navier-Stokes (NS) solutions and expand the scope of its application, demonstrating its applicability in the correlation/prediction of velocity and enthalpy profiles as well as distribution functions for a monatomic gas.					
14. SUBJECT TERMS					
17. SECURITY CLASSIFICATION OF REPORT UNCLASSIFIED				18. SECURITY CLASSIFICATION OF THIS PAGE UNCLASSIFIED	
19. SECURITY CLASSIFICATION OF ABSTRACT UNCLASSIFIED				20. LIMITATION OF ABSTRACT BAR (SAME AS REPORT)	
15. NUMBER OF PAGES 32				16. PRICE CODE	

93-16799



AFOSR Contract No. 91-0104

To Extend the Thirteen-Moment Theory and Its Application to Problems in Rarefied Hypersonic Flow

Principal Investigator: H. K. Cheng

Department of Aerospace Engineering
University of Southern California
Los Angeles, California 90089-1191

18 May 1993

Final Technical Report

Period: 12/01/90-05/31/93

Accession For	
NTIS	CRA&I <input checked="" type="checkbox"/>
DTIC	TAB <input type="checkbox"/>
Unannounced <input type="checkbox"/>	
Justification	
By	
Distribution /	
Availability Codes	
Dist	Avail and/or Special
A-1	

Air Force Office of Scientific Research
Bolling Air Force Base
Washington, DC 20332-6448

CONTENTS

1	Introduction	3
2	Review of Research Development and Results	3
2.1	The Kinetic-Theory Based Shock-Layer Approximation	4
2.2	Quasi 1-D Shock Structure	7
2.3	Computational Studies: PNS and Other Thin-Layer Approximations	13
2.4	Time-Accurate NS Calculations	18
3	New and Unresolved Issues	25
3.1	Gas-Kinetic Based Extension of the Continuum Model	25
3.2	Use and Implementation of PNS Equations; Görtler Vortices and Upstream Influence	26
3.3	Flap/Aileron Effectiveness: Time-Accurate NS and DSMC Calculations . . .	26
3.4	Quasi-1-D Shock Structure	27
3.5	Thermo-Chemical Nonequilibrium in Rarefied Hypersonic Flow	27
3.6	Hypersonic Boundary Layer Instability: Power-Law Shock and Görtler Insta- bility	28
4	Conclusion	28
5	Publications and Documented Works Resulting from the Present Support	29
6	References	30

Summary

Research development and results on rarefied hypersonic flow under AFOSR support (contract 91-0104) covering the period 12/01/90-01/15/93 is reported.

The theoretical development and supporting particle-simulation (DSMC) and other computational studies carried out during the past two years have strengthened the principle for correlating a flow far from translational equilibrium with the Navier-Stokes (NS) solutions and expand the scope of its application, demonstrating its applicability in the correlation/prediction of velocity and enthalpy profiles as well as distribution functions for a monatomic gas.

Analyses of the shock-transition zone of an oblique, curved bow wave have been made via a quasi-1-D model consistent with the thin shock-layer concept in two parallel approaches: (a) a combined Mott-Smith and Grad moment method, which may be referred to as a *multi-mode* method; (b) quasi-1-D DSMC model.

In support of this effort, CFD codes have been developed from parabolized Navier-Stokes (PNS) equations, from a time-accurate, predictor-corrector NS method, and more recently, from a time-accurate thin-layer NS equations. Apart from furnishing NS data for the correlation studies uncovering a number of unique features, the computational study demonstrates

that the correlation principle applies also to slender/thin obstacles which were not considered in the original theory, and that a strip method is applicable to flows about a wide class of flat lifting surface. The latter leads to a new approach for generating "bridging function" of interest to hypersonic vehicle design study.

Adding credence to the present approach based on Grad's 13-moment equations are two studies made to demonstrate its relative merit over that based on Burnett equations.

1 Introduction

The Direct Simulation Monte Carlo (DSMC) and other particle simulation calculations have been widely adopted in most rarefied gasdynamic studies to date (e.g. Refs. 1, 2). These simulation techniques can produce solutions in the transition range even in flow regimes near translational equilibrium, but are far more costly than the Navier-Stokes (NS) solvers (e.g. Ref. 3). Among the limitations which handicap the use of particle simulation methods as an aerothermodynamic prediction tool is that the *cell size* must be an order comparable to the *mean-free path*, requiring unmanageable computer resources for its application near the continuum end of the transition regime.

Under NASA-DOD (NAGW-1061) and AFOSR (88-0146, 91-0104) joint support, a development extending the continuum model has been undertaken to address an important class of rarefied hypersonic flows in which, unlike in the Chapman-Enskog [4,5,6] and Burnett theory [7], the departure from local translational equilibrium is *not* required to be strictly small. The gas-kinetic basis of this development is Grad's [8] 13-moment equations, simplified under the shock-layer formalism familiar in the hypersonic flow theory [10]–[12]. As the goal set forth in our earlier program, the major objective is to provide insight and a framework to facilitate physical understanding of the highly nonequilibrium hypersonic flow. The following section will review principal results obtained and report recent developments under the support of AFOSR Math. Information Sci. Program during the past two years. The new and remaining issues are noted/discussed in Section 3.

2 Review of Research Development and Results

The earlier works serving as background of the current research were presented in the cited references [9]–[11] and were summarized and explained in the proposal for a program "To Extend the Thirteen-Moment Theory and Its Application to Problems in Rarefied Hypersonic Flow" submitted to Dr. A. Nachman of the AFOSR in early 1990. Results from the present program generated during the last two years have been presented in an AIAA paper [12], an invited paper in the 9th International CFD Symposium [13], an invited paper in the IUTAM Aerothermochemistry and Hypersonic Flow Symposium [14], and a paper accepted for publication in *AIAA J.* [15]; also one manuscript submitted to *AIAA J.* [16] and another to the *J. Fluid Mechanics* [17]. These and related aspects of rarefied hypersonic flow research are reviewed in an article by the PI in *Annual Review of Fluid Mech.* [19]; also in a white paper on nonequilibrium hypersonic flow research, documented as a report USCAE 151 [20]. Results also have been documented in two reports (see Refs. [16, 17]) and in a publication

under the Pitman Research Notes Math. Series [61]. An invited paper on the subject is scheduled to be presented at the International Workshop on Advances in Modeling of Aerodynamic Flows, to be held at Miedzyzdrze, Poland, July 12-14, 1993 [18]. A Ph.D. thesis [21] and a *J. Fluid Mech.* manuscript [22] are due to be completed in August 1993.

The following will report the work under this program and discuss the research results.

2.1 The Kinetic-Theory Based Shock-Layer Approximation

Grad's thirteen (13)-moment equations fail to yield solution structure to a plane shock for Mach number higher than 1.65, as is well known [23,24]. The present study concerns, however, their applications and extension to the flow behind/downstream of the shock structure, particularly the relatively thin region between a strong shock and a solid body surface, called the "shock layer".

Translational Nonequilibrium in Fully Viscous Shock Layer

The rarefied hypersonic problems of interest occur in a domain where the rarefaction degree (or the flight altitude) is high enough that the shock-layer must be considered *fully viscous*, yet low enough that a shock structure distinct from the shock layer can still be identified. The fully viscous condition necessarily implies a significant departure from translational equilibrium, as noted in Ref. [10,11].

Reducing Grad's Equations: A Correlation Principle

Grad's 13-moment equations may then be simplified under the shock-layer formalism in this case, i.e., assuming the negligibility of the streamwise molecular transports and a small $\epsilon \equiv (\gamma - 1)/2\gamma$, where γ is the specific-heat ratio. We shall return to the question on adequacy of this assumption for a monatomic gas later. An important consequence of this simplification is reduction of the constitutive relations (of the principal deviatorial stress and heat-flux components) to a form amendable to further reduction to a thin-layer NS system (via von Mises or Dorodnitsyn variables). It renders possible the correlation of a shock-layer flow far from translational equilibrium with that based on the NS equations. This development and the correlation principle have been elucidated and demonstrated with extensive comparison of the NS and particle-simulation calculations in Refs. [10]–[15] for a nonaligned flat plate, where more comprehensive presentation of the theory and its requirements have been given. More recent calculations extended to include a lower attack-angle range, to be included in Refs. [21,22], show that more effective flow-field correlation can be found at plate attack angles $\alpha = 20^\circ$ and 30° where the nonequilibrium parameter P_{22}/p differs more markedly from unity.

Shock-Structure Bypass

Another key to this 13-moment based theory is the availability of the boundary condition at the shock-layer's *outer* edge, which allows solution to the shock-layer problem without the need of a full knowledge of the shock structure. These outer boundary conditions take

Thin-Layer Approximations:
 $\Delta/L \ll 1, \Delta_s/L \ll 1$

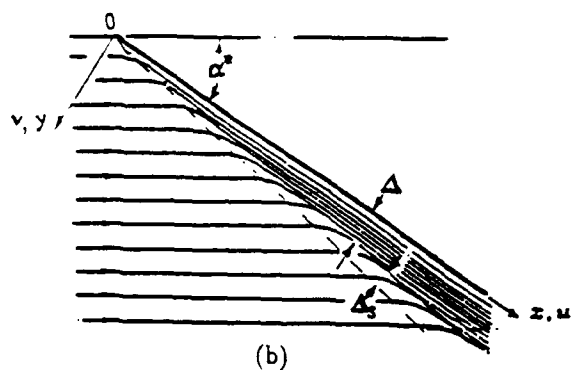
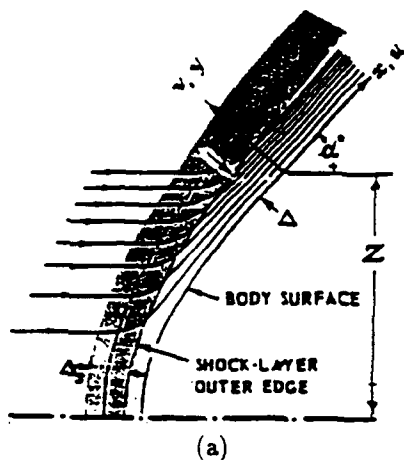


Fig. 1

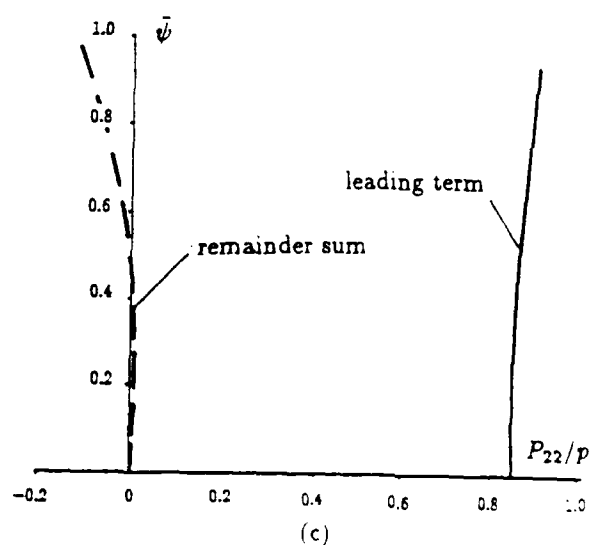
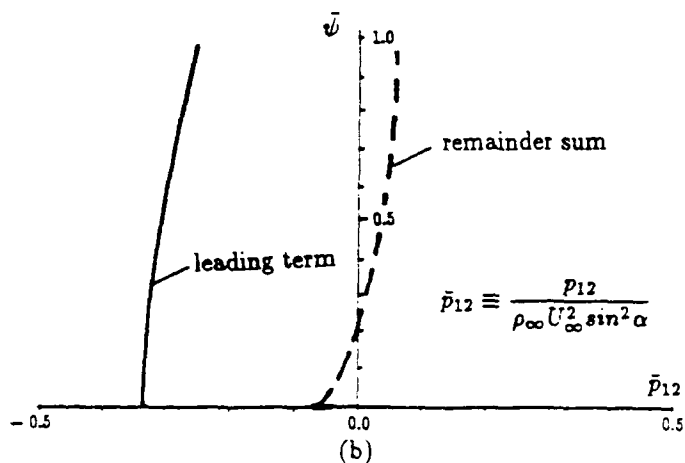
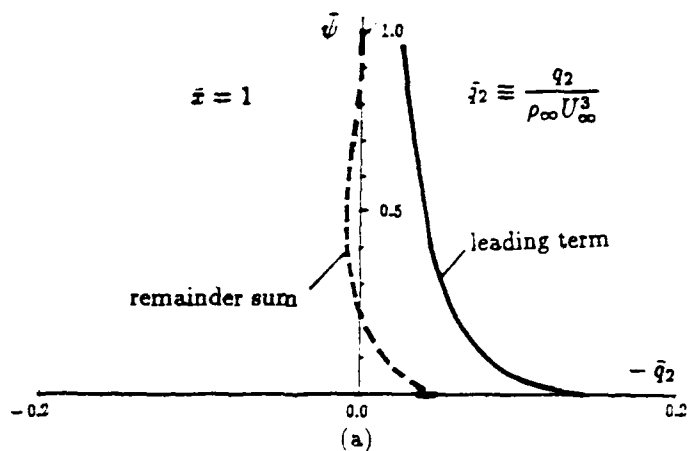


Fig. 2

the form of corrections to the Rankine-Hugoniot (shock) relation, very much like wall-slip and temperature-jump corrections at a solid surface. They have been therefore referred to as *shock-slip* effects. As long as the shock thickness is small on a global length scale, the corrections/effects in question are independent of the gas-kinetic detail of the shock structure [10–12].

Wall Slip and Strong Wall Cooling

For *small* slip corrections Grad's wall model in his 13-moment theory yields essentially the same velocity slip and temperature jump in the classical theory which amount to a relative order

$$\sqrt{\epsilon T_w/T_0}$$

under the present formalism. Thus, apart from raising the density level in favor of the thin shock-layer approximation, strong wall cooling ($T_w/T_0 \ll 1$) of relevance to hypersonic flight makes the wall-slip effect unimportant. It also simplifies the application of the correlation principle through the elimination of the wall slip as an important parameter in the correlation [10]–[12].

The Proper Type and Number of Boundary Conditions

As shown by Grad [8], by considering the number of characteristics of his (unsteady) 13-moment equations which can reach a solid boundary, the type and number of boundary conditions on the solid boundary are found to be the *same* as the wall-slip conditions of the NS system. The conclusion is made more evident in the present framework by virtue of the correlation principle. Unlike the Burnett equations, the issue on the sufficiency of the NS type boundary conditions to the solutions' unique determination remains open. This issue with the Burnett equations will be addressed further later.

Errors of the Shock-Layer Formalism and in the 13-Moment Equations

Underlying this gas-kinetic based shock-layer theory is the greatly simplified constitutive relations which are subject to errors from the thin-layer approximation and the formalism treating $\epsilon \equiv (\gamma - 1)/2\gamma$ as a small quantity. It is essential to assess the remainders in the principal stress and heat-flux components which are used in the (leading-order) theory. In Figs. 2a,b,c, the profiles of the tangential stress p_{12} , the normal component of the heat flux q_2 , and the ratio of pressure tensor component $P_{22} \equiv p + p_{22}$ to the thermodynamic pressure p in a fully viscous shock layer (FVSL) on the windward side of a flat plate at 40° attack angle were computed from the theory for a Maxwell gas. The results are shown in Figs. 2a,b,c as functions of a normalized stream function $\bar{\psi}$ (in solid curves), while their remainders in the 13-moment equations are computed and shown also in each figure (in dash curve). Here, the remainders are seen to be indeed numerically small, and the error in the reduced constitutive relations may thus be considered unimportant.

Errors are introduced in moment equations themselves from the approximation to the velocity-distribution function f required for the system closure. These errors can be traced to the collision integral and from terms involving the higher moments. For a Maxwell gas, the collisional terms in the moment equations is exact (has no error), irrespective of the form of " f ". For a non Maxwell gas, however, these errors are very limited in magnitude, according to a detailed examination based on Grad's early analysis [8] reported by H. T. Yang [17]. The source of errors in the constitutive relations therefore occur mainly through approximating the " f " in the higher moments for closure. An example of the distribution function of the 13-moment theory at various locations inside a fully viscous shock layer has been illustrated in Ref. 12 (Sec. 4 and Fig. 13 therein). The f -distributions are well behaved, except in the immediate vicinity of the wall, where a small velocity domain with negative " f " can be found in the more rarefied flow region upstream. This inadequacy of the assumed form of " f " is not unexpected for the case of a strong wall cooling with high local heat flux q_2 and low wall temperature T_w , and determine the departure from the local Maxwellian through q_2/pRT [12] which may be referred to as the "cold-wall anomaly". But its effects on the heat flux and skin friction are small, as good agreement of the theory with DSMC calculations and experiments have indicated. In this regard, the detailed comparisons with particle simulation methods in surface properties made in Refs. [10]-[15] are therefore important.

Detailed Comparison with DSMC Calculations

A more detailed comparison of Grad's distribution function using coefficients determined from the FVSL solution with that sampled from the (2-D) DSMC calculations can provide much insight to the nature of the rarefied hypersonic flow and lead to an improvement of the theoretical model. Figures 3(a)-3(f), 4(a)-(f) present results of such a comparison, where the "parallel distributions" $f_{||}$ and the "perpendicular distributions" f_{\perp} , defined here as

$$f_{||} = \int \int f d\eta d\zeta, \quad f_{\perp} = \int \int f d\xi d\zeta, \quad (1)$$

from the two sets of calculations are shown and compared at three (lower, middle and upper) levels of the shock layer for two values of

$$\bar{x} \equiv \epsilon \frac{\rho_{\infty} U_{\infty} x}{\mu_0} \left(\frac{\mu_0 T_{\infty}}{\mu_{\infty} T_0} \right) \sec \beta \quad (2)$$

corresponding to two different distances from the apex. For the present purpose, \bar{x} may be taken as a rescaled, local Reynolds number, the reciprocal of which indicate the order of $|p_{ij}/p|$, hence the degree of translational nonequilibrium. The results at the station $\bar{x} = 1$ are shown in Figs. 3, where the parallel and perpendicular distribution are presented in (a)-(c) and in (d)-(f), respectively. Except for the spike-like feature in the DSMC data noticeable at the upper level (outer edge), and the higher value near the peak at the level next to the wall, the distributions assumed by the 13-moment model (in open circles) and obtained from DSMC calculations (in solid curves) are generally in accord. The spike is identified with the remainder of a more pronounced feature present in the high Mach-number shock

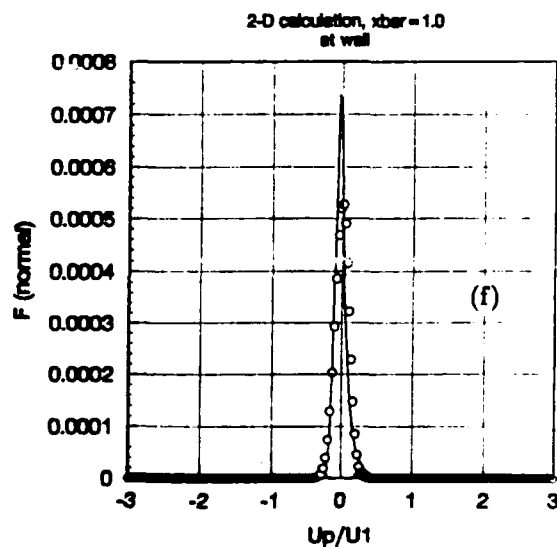
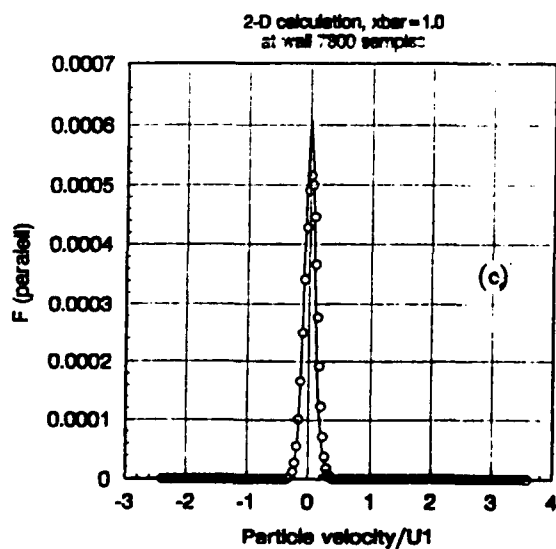
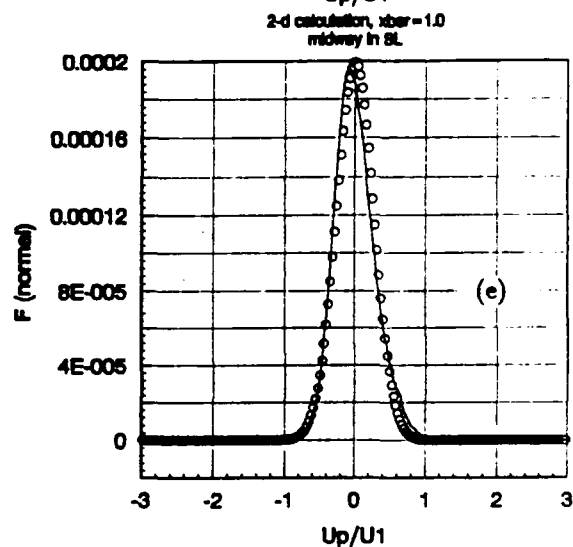
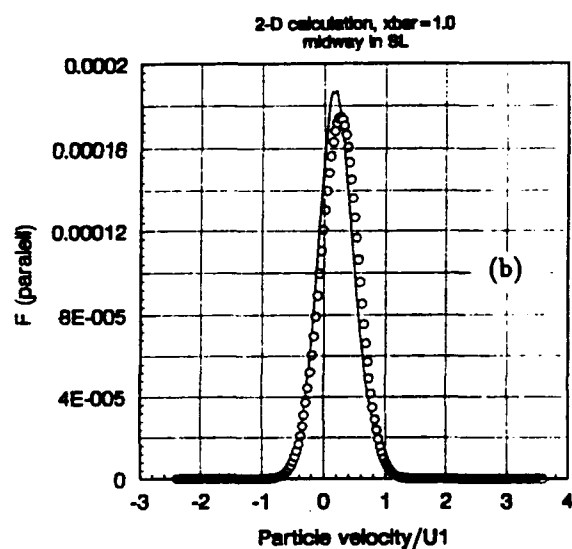
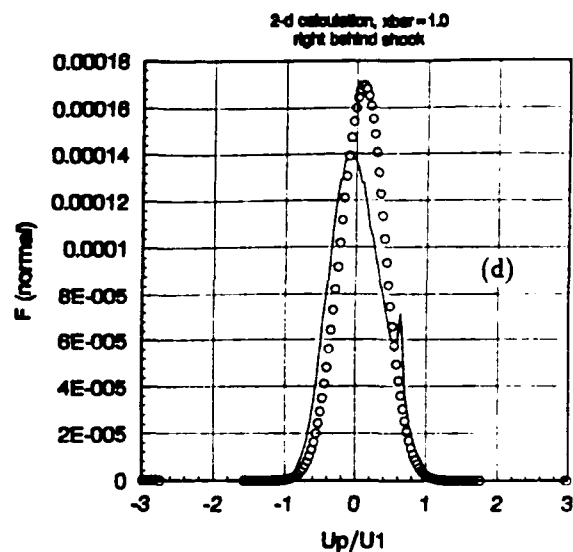
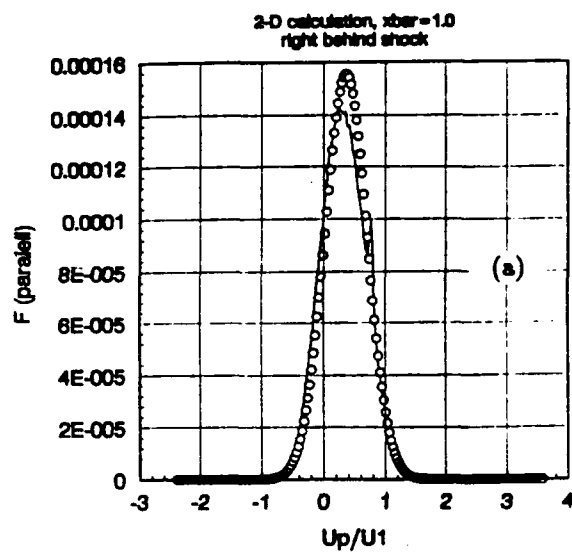


Fig. 3

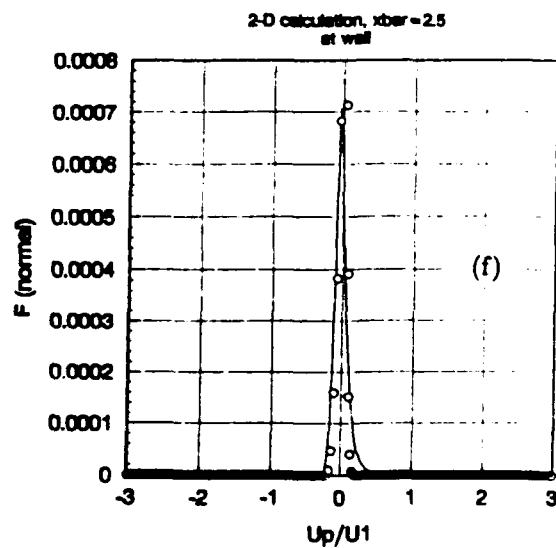
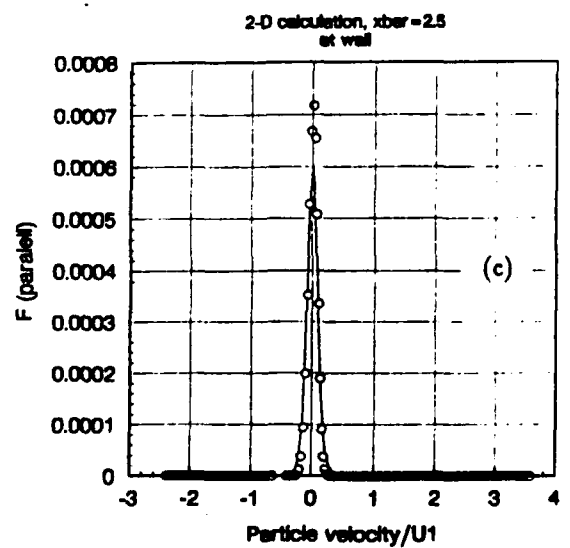
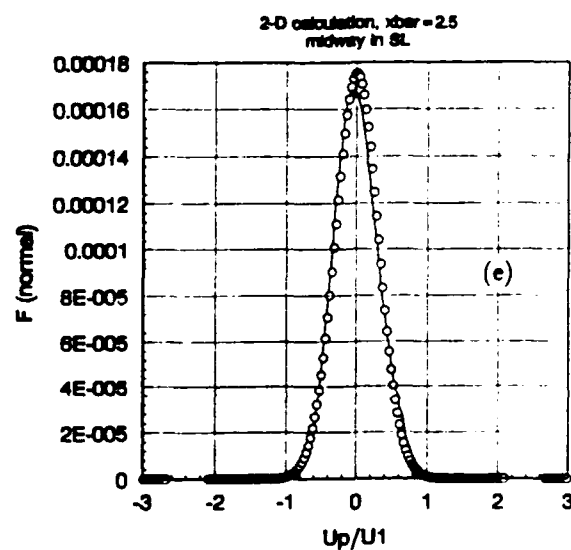
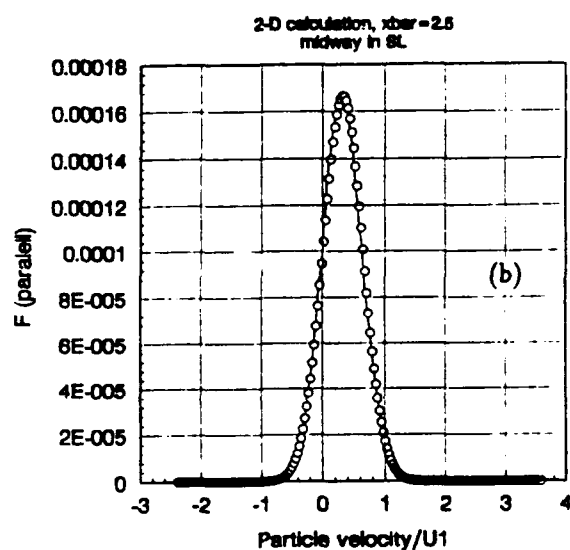
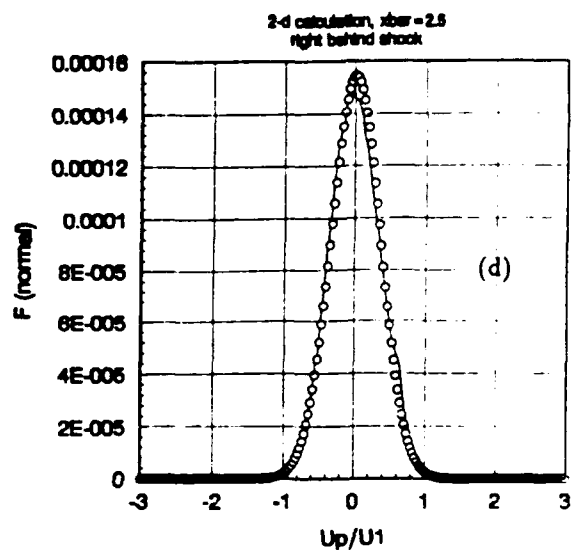
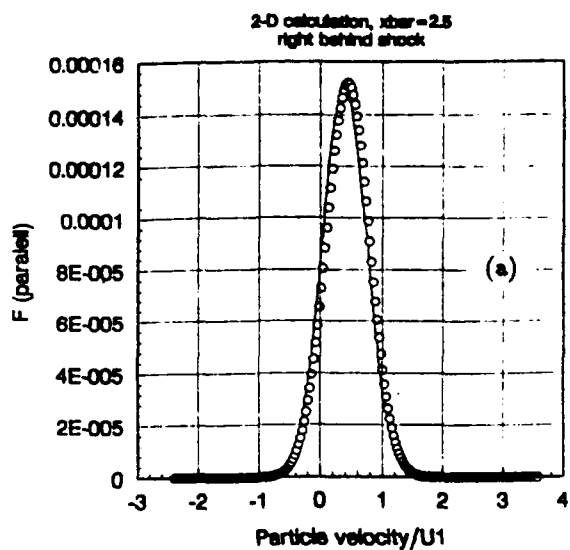


Fig. 4

familiar from experiment and DSMC analyses [26], which signifies the persistence of the upstream influence. The discrepancy near the wall may be related to the cold-wall anomaly mentioned, although negative values in f_{\perp} and f_{\parallel} are not found. These features cannot affect significantly the macroscopic properties and diminish at the more downstream stations, as shown in Figs. 4(a)-(f) for $\bar{x} = 2.5$. The foregoing comparison adds credence to Grad's 13-moment theory *behind* the shock, which is central to the present development; it also reveals the persistent nature of the upstream state which must be dealt with in future improvement of the moment (transfer-equation) method. We shall return to this spiky feature in the shock structure problem later, which represents an all important issue in the modeling of the shock-transition zone.

Three-Dimensional Extension: Strip Method

The 13-moment based FVSL theory and its correlation principle has been extended to 3-D in a form rather similar to the classical 3-D boundary layer theory [12]-[14]. Implicit is that the transverse tangential (spanwise) length scale cannot be too small compared to the streamwise length scale. For a flat-bottom lifting surface, or a flat plate at incidence, of arbitrary planform, a *quasi*-2-D theory allowing the shock slips is found to be applicable along each (projected) *streamwise strip* [12]-[14]. This strip method was tested against a 3-D PNS calculation for flat-plate delta wings and proved to be adequate (see §2.3 on supporting equations and code developments below). Its application would lead one to anticipate a significant dependence of the aerodynamic properties on the planform geometry, owing to the fact that local skin friction will depend on the distance from the leading edge along the strip in question. It turns out that the lift-to-drag ratio, L/D , in this case, has a strong preferential dependence on the span-averaged chord (SAC) and is surprisingly insensitive to the planform variation [12]-[14]. To test this SAC rule, the strip method was applied to ten (10) dissimilar planforms and sizes for flat plates at 20° and 40° attack angles. With the SAC replacing the distance x on a 2-D plate, the L/D of these lifting surfaces (omitting the contribution on the suction side) are correlated in Fig. 5 as a function of the rescaled Reynolds number \bar{x} of Eq. (2), which fits well with the 2-D results from DSMC and FVSL calculations. The study therefore furnishes a single "bridging function" spanning the transition range for a wide class of flat lifting surfaces (for each attack angle), which is given simply here by the correlated 2-D data curve. To establish a firmer base, data from genuine 3-D calculations by DSMC and NS methods should be included in the correlation study.

2.2 Quasi 1-D Shock Structure

The outer-boundary conditions involving shock slips in the foregoing development allow one to bypass the shock-structure problem. Implicit is the *quasi*-1-D assumption which follows from the thin-layer approximation and has been used earlier by the PI [27,28] in analyzing the (oblique) NS shock structure (and its matching with the downstream shock-layer flow). It is therefore of interest to seek a *quasi*-1-D shock-structure based on the particle-simulation method and on other gas-kinetic models such as one based on an improved version of the moment method.

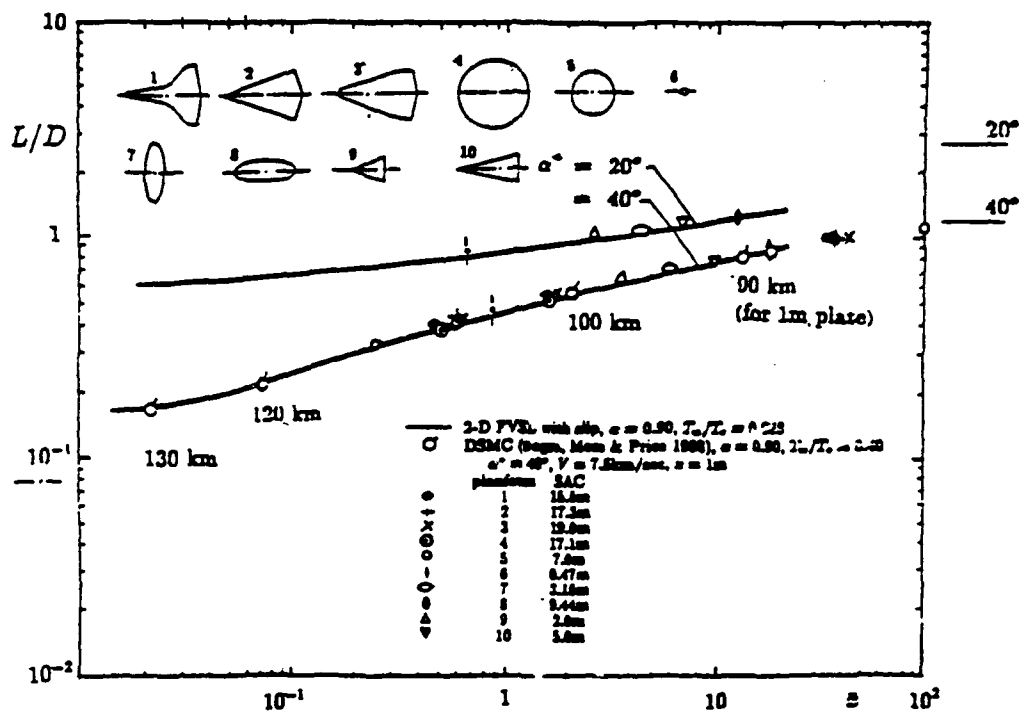


Fig. 5

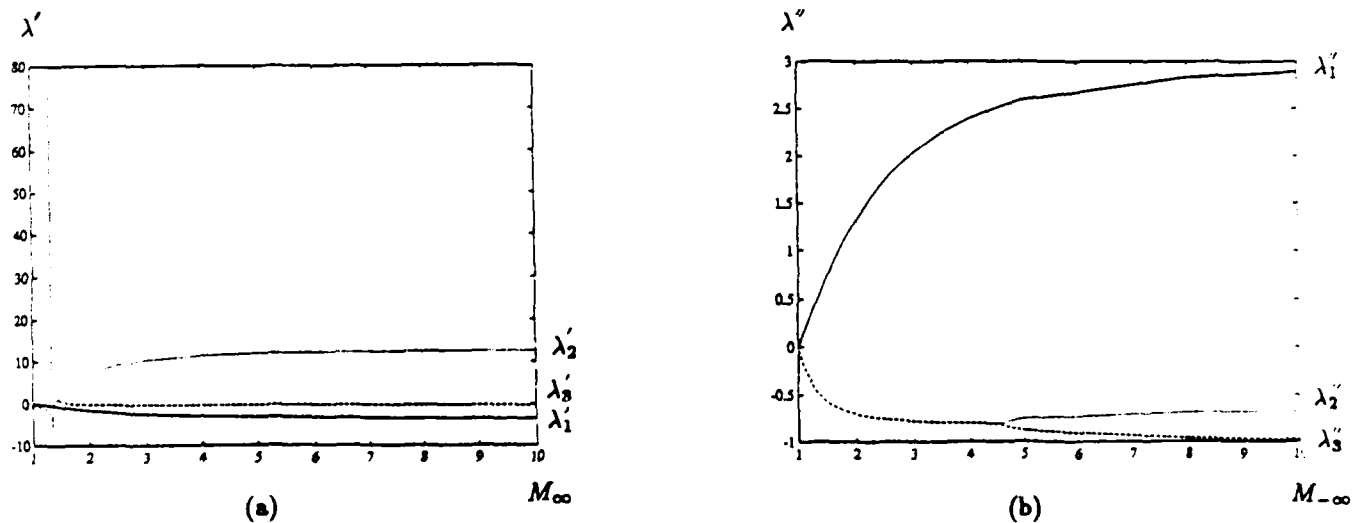


Fig. 6

DSMC Study

The *quasi*-1-D shock-structure problem of interest differs from the classical plane shock problem mainly in the presence of the nonvanishing heat-flux and deviatorial stress (pressure-tensor) components at the downstream control surface identified with the FVSL's outer edge. Unlike the standard DSMC procedure in which the shock structure is allowed to drift freely through the calculation domain, the downstream control boundary is fixed with the last downstream cell. The viability of the procedure using a fixed downstream boundary was tested in a numerical DSMC experiment. Here an arbitrary downstream boundary is chosen at a station interior of a stationary plane shock. Velocity of the particles which cross the boundary are stored in a file so that a downstream distribution function can be used to replace the equilibrium Maxwellian distribution function at the far downstream. In any case, the sampled distribution function is applied to the downstream control surface and the same stationary DSMC solution (upstream of the control surface) is recovered with this arrangement, which is rather insensitive to the initial data used.

The second issue concerning the *quasi*-1-D shock structure is the fulfillment of the mass, momentum and energy conservation laws. In the specification of the downstream boundary conditions for the *quasi*-1-D shock, half of the velocity space of the 13-moment distribution is used for the purpose of particle velocity sampling. Expressible entirely in terms of local flow state, namely k_{ij} , q_i and etc., the 13-moment distribution function is seen to be quite independent of the upstream high speed particles. Indeed, the velocity distribution functions obtained from the 2-D DSMC calculations at locations behind the shock are noticeably different from that of 13-moment. There is no assurance that the conservation laws are adequately satisfied. The flux imbalance is believed to be the main cause for failing to reach a steady state, and ways to implement the flux conservation at the downstream control surface is being considered.

It is interesting to note the persistent influence of the upstream state reflected by the pronounced spiky, bimodal-like distribution appeared in $f_{||}$, was brought out in Ref. [26] and discussed also in Ref. [12] for a plane normal shock. An important feature brought out by our DSMC calculations in the course of the present study is the surprisingly early decay of this spiky bimodal-like feature towards the downstream end where most macroscopic properties, such as density, velocity, and temperature, have not quite reach their respective downstream/terminal values. This appears to be consistent with the lesser prominence of the bimodal-like features in the shock layer at $\bar{x} = 1$ (Fig. 3) and its total disappearance in the shock layer at $\bar{x} = 2.5$ (Fig. 4).

Analyses with Higher Moments/Multi-Modal Approach

Analyses of shock structure using equations higher than the 13-moment levels was initiated early in the program. The work was motivated by the pronounced spiky feature brought out in Ref. [26], reminiscent of the Mott-Smith's bimodal distribution [29], which is not describable by solution to the 13-moment equations in Grad's original form. It is essential to point out that the additional moments are introduced here not as a straightforward improvement of Grad's Hermite-polynomial expansion of the distribution function " f ", but,

rather, Grad's form of f is to be used as terms *filling the gap* between the humps of the Mott-Smith type bimodal distribution. The following highlights the essence and issues of this development which may be called a multi-modal approach and will be extended subsequently to complement and improve the 13-moment based fully viscous shock layer (FVSL) theory.

Need of Higher Moments and Other Distinct Modes As an improvement of the 13-moment equations, the *thirteen* moments in Grad's original system will be kept. The moments represent the macroscopic quantities of engineering interest: density ρ , velocity components u_i , pressure tensor P_{ij} , and heat flux q_i (or $S_i = 2q_i$, $i, j = 1, 2, 3$). One or two more moments higher than the thirteenth will therefore be added to accommodate the persistent influence of the upstream and downstream states in the Mott-Smith sense. We assume for the distribution function the form

$$f = \alpha' e^{-\beta' c'^2} + \alpha'' e^{-\beta'' c''^2} + \alpha e^{-\beta_k c_k^2} (1 + A_{mn} c_m c_n + B_m c_m + C_m c_m c^2) \quad (3)$$

where $c_i \equiv \xi_i - u_i$ is the thermal/peculiar velocity component, $\beta_i \equiv (2RT_i)^{-1}$ with T_i being the temperature associated with the i th thermal velocity component

$$2RT_i = \frac{1}{\rho} \int \int \int c_i^2 f dc_1 dc_2 dc_3, \quad (4)$$

$\beta \equiv (2RT)^{-1}$ with T being the (translational) temperature

$$2RT = \frac{1}{\rho} \int \int \int c^2 f dc_1 dc_2 dc_3; \quad (5)$$

the single-prime and double-prime superscripts signifies the upstream and downstream states, respectively; and $c^2 = c_k c_k$; repeated indices is understood as summation. Except for replacing βc^2 in $e^{-\beta c^2}$ by $\beta_k c_k^2$, the last group of terms is comparable to Grad's original form. For clarity, we note the relations/definitions

$$\begin{aligned} \rho &\equiv \int \int \int f d\underline{c}, & u_i &= \frac{1}{\rho} \int \int \int f \xi_i d\underline{c}, \\ P_{ij} &\equiv \int \int \int c_i c_j f d\underline{c}, & S_{ijk} &\equiv \int \int \int c_i c_j c_k f d\underline{c} \\ S_i &\equiv S_{ikk}, & d\underline{c} &\equiv dc_1 dc_2 dc_3 \end{aligned} \quad (6)$$

The fifteen coefficients $\alpha, \alpha', \alpha'', A_{ij}$, etc. can be expressed in terms of the *thirteen* macroscopic properties mentioned as well as *two* parameters controlling the relative importance of the Mott-Smith terms

$$\theta' = \left[\frac{\beta_1 \beta_2 \beta_3}{(\beta')^3} \right]^{1/2} \frac{\alpha'}{\alpha}, \quad \theta'' = \left[\frac{\beta_1 \beta_2 \beta_3}{(\beta'')^3} \right]^{1/2} \frac{\alpha''}{\alpha} \quad (7)$$

Among the fifteen PDEs needed, thirteen have been obtained in Grad's [8], taken from the zeroth, ξ_i , $\xi_i \xi_j$, and $\xi_i \xi_k \xi_k$ -moments of the Boltzmann equation. Before deciding on the additional equations, an appropriate choice for the new higher moments must be considered. Consider the complete set of the ten (10) third-order moments

$$\begin{array}{ccccccc}
S_{111} & - & S_{122} & - & S_{133} & & \\
& \ddots & & & & & \\
S_{211} & - & S_{222} & - & S_{233} & \text{and} & S_{123} \\
& & \ddots & & & & \\
S_{311} & - & S_{322} & - & S_{333} & &
\end{array} \quad (27)$$

of which the sum of each row in the 3×3 array has already been utilized in defining the heat flux, i.e. $S_i \equiv S_{ikk}$ in Eq. (6). One of the new moment can be taken as the sum along the diagonal $\sum_k S_{kkk}$, i.e.,

$$S_{111} + S_{222} + S_{333}, \quad \text{or} \quad \sum_k \int \int \int c_k^3 f d\mathbf{c} \quad (28)$$

and the remaining moment could have been obtained from the other diagonal $S_{311} + S_{222} + S_{133}$. However, the last choice would lead to a redundancy, at least for the important 1-D problem of shock structure. This is because in the latter case, all elements S_{ijk} vanish except those on the first row, and $S_{311} + S_{222} + S_{133} = S_{133}$, but S_{133} has already been determined by $S_{133} = S_{122} = \frac{1}{2}(S_1 - S_{111})$ in this case. Any other combination of third-order moments, including S_{123} cannot yield an independent new moment for 1-D applications. Thus the present study shows that in order to determine α' and α'' in Eq. (3) a fourth-order moment, which is beyond that of Grad's twenty moments [8], becomes necessary. Equations needed for the fourth-order moment have been worked out in detail by Ikenberry & Truesdell [30] corrected/updated by Perminov & Frilander [31]. The simplest moment of this order/level is evidently

$$P_4| \equiv \int \int \int c^4 f d\mathbf{c} \quad (29)$$

This PDE system cannot be closed without expressing certain higher-order terms (such as some of S_{ijk} and Q_{ijkl}) in terms of the lower moments, as is understood.

A 14-Moment System A complete system of fifteen moments which includes $\sum_k S_{kkk}$ and $P_4|$, was studied. There is a peculiar upstream behavior common to solutions of the moment equations involving Mott-Smith type distributions, such as that of Eq. (3), of which the analytical difficulty is compounded by the fourth-order moments. The following describes an alternative analysis using a total of fourteen moments, which avoids the fourth-order moments but retains the distinct bi-modal character. This is accomplished by assuming an algebraic relation between α' and α'' , which satisfies the requirement that α'' vanishes where α' tends to the upstream equilibrium value, and α' vanishes where α'' takes on a downstream equilibrium value. This also implies that the Grad-type distribution in Eq. (3) is now simply relegated a role to filling the valley between the humps of the Mott-Smith mode. Not much loss in generality results from this assumed relationship of α' and α'' , since the Grad-type distribution is capable to reproduce completely the equilibrium distributions upstream and downstream and to provide effectively the necessary corrections to α'' which is itself rather smooth. The desired behaviors can be conveniently achieved through imposing

a relation between the two parameters arising from normalization of the PDEs and algebraic relations among the moments:

$$\varphi' \equiv \frac{\theta'}{1 + \theta' \left(1 + \frac{\sigma'_1}{2}\right) + \theta'' \left(1 + \frac{\sigma''_1}{2}\right)}, \quad \varphi'' = \frac{\theta''}{1 + \theta' \left(1 + \frac{\sigma'_1}{2}\right) + \theta'' \left(1 + \frac{\sigma''_1}{2}\right)} \quad (30)$$

where σ'_1 is independent of θ' and vanishes when $\beta_i \rightarrow \beta'$, $u_i \rightarrow u'_i$; σ''_1 is same as σ' with all primes in the superscripts replaced by double primes. Now, we can take

$$\varphi' + \varphi'' = 1 \quad (31)$$

or more generally

$$\varphi' = (1 - \varphi'')P(\varphi'') \quad (32)$$

where $P(\varphi'')$ is a polynomial with $P(0) = 1$. Equation (31) is preferred for its simplicity. It follows that if $\varphi' \rightarrow 1$ upstream, then φ'' , θ'' , α'' as well as α will vanish there. Similarly if $\varphi'' \rightarrow 1$ downstream, then φ' , θ' , α' as well as α will vanish. With the relation (31), we need only one more moment to accommodate φ' or φ'' , which is the diagonal sum $\sum_k S_{kkk}$ of Eq. (28). The governing PDE needed may be obtained from the $\sum_k \xi_k^3$ -moment of the Boltzmann equation, which can be found among Grad's twenty (20)-moment equations. The 14-moment system with Eq. (31) should remain applicable even if there exists no downstream equilibrium state; in this case, φ' needs not vanish on a boundary.

1-D Shock Structure For the 1-D shock-structure, the 14-moment equations with (2.1.31) or (2.1.32) can be reduced to a system of three ordinary differential equations (ODE). In normalized form, they are

$$\frac{d}{d\eta} [3(1 + \bar{p}_1)\bar{u} - 2\bar{u}^2 + \bar{S}_{111}] = -(P - \bar{p}), \quad (33)$$

$$\frac{d}{d\eta} [(1 + 5\bar{p}_1)\bar{u} + 3(1 + \bar{p}_1)\bar{u}^2 - 3\bar{u}^3 + 2\bar{u}\bar{S}_{111} + \bar{u}\bar{S} + \bar{Q}_{11kk}] = -\frac{2}{3}\bar{S} - 2\bar{u}(P - \bar{p}), \quad (34)$$

$$\frac{d}{d\eta} [2(1 + \bar{p}_1)\bar{u}^2 - \frac{5}{3}\bar{u}^3 + \frac{4}{3}\bar{u}\bar{S}_{111} + \frac{1}{3}\bar{Q}_{1111}] = -\frac{1}{2}\bar{S}_{111} + \frac{1}{6}\bar{S} - \bar{u}(P - \bar{p}) \quad (35)$$

where $\bar{p}_1 = 3/5M_1^2$ and

$$\bar{u} \equiv \frac{u}{u_1}, \quad \bar{S} \equiv S_1/\rho_1 u_1^3, \quad \bar{S}_{111} \equiv S_{111}/\rho_1 u_1^3, \quad \bar{p} \equiv p/\rho_1 u_1^2$$

$$P \equiv P_{11}/\rho_1 u_1^2, \quad \bar{Q}_{1111} \equiv Q_{1111}/\rho_1 u_1^4, \quad \bar{Q}_{11kk} = Q_{11kk}/\rho_1 u_1^4$$

$$\xi \equiv x/\lambda_1, \quad \bar{u} \equiv \mu/\mu_1, \quad \eta \equiv \frac{\rho_1 u_1 \lambda_1}{\mu_1} \int_0^{\bar{p}} \frac{\bar{p}}{\bar{\mu}} d\bar{\xi}$$

The unknowns in the above ODEs can be considered as \bar{u} , \bar{S} and φ' , with \bar{S}_{111} and $(P - \bar{p})$ eliminated by their known algebraic relations to \bar{u} , \bar{S} , φ' and φ'' . The four-order moments \bar{Q}_{11kk} in Eq. (34) and \bar{Q}_{1111} in Eq. (35) are evaluated with the assumed/approximate

distribution f of Eq. (3) in terms of $\alpha, \alpha', \alpha'', A_{mn}$ etc., which are in turn expressed in terms of $\bar{u}, \bar{S}, \bar{S}_{111}, \varphi', \varphi''$ etc. In this manner, these three ODEs could be regarded as the first three equations of the system for $\bar{u}, \bar{S}, \varphi'$ and φ'' . The additional ODE is now unnecessary on account of Eq. (31) or (32). In passing, in Grad's system which consists of only Eqs. (33) and (34), an approximation relation of \bar{S}_{111} to \bar{u} and \bar{S} was used for closure, which is treated exactly here.

The upstream boundary conditions are provided by, $\eta \rightarrow -\infty$

$$\bar{u} \rightarrow 1 \quad \bar{S} \rightarrow 0 \quad \varphi' \rightarrow 1 \quad (\text{and } \varphi'' \rightarrow 0). \quad (36)$$

Critical is the answer to the question whether Eqs. (33)–(35) admit a solution which can approach the upstream limit Eq. (36) smoothly. It is in answering this question in the phase plane that Grad found the failing of his 13-moment equations at M_1 beyond 1.65. For the present system with more than two unknown variables, the question may still be answered by seeking directly a perturbation solution in η .

An interesting property of Eqs. (33)–(35), as the first three equations governing the four unknowns ($\bar{u}, \bar{S}, \varphi'$ and φ''), should be brought out before going on to solve them for the three unknowns (\bar{u}, \bar{S} and φ'). Namely, in expanding the three ODEs about the upstream state, neither φ' nor $d\varphi'/d\eta$ appear in the linearized equations. These equations may therefore be decoupled from the (unwritten) fourth equation and yield the departure solution behavior for \bar{u}, \bar{S} and φ'' . Similarly expanding these three equations about the downstream state, neither φ'' nor $d\varphi''/d\eta$ can be found in the linearized equations. Hence the additional equation from the fourth-order moment would (assume) the burden of providing departure solutions for φ' upstream and for φ'' downstream. The analysis also shows that if α'' or φ'' were identically zero in the outset, these three equations would lead to a redundancy in the determination of \bar{u} and \bar{S} .

For the 14-moment based system with Eqs. (33)–(35) at hand, we simply seek solution to the linearized homogeneous system for $\eta \rightarrow -\infty$

$$\begin{pmatrix} \bar{u} - 1 \\ \bar{S} \\ \varphi'' \end{pmatrix} = \begin{pmatrix} A \\ B \\ C \end{pmatrix} e^{\lambda' \eta}$$

or

$$(\bar{u} - 1, \bar{S}, \varphi'')^T = (1, B', C')^T e^{\lambda'(\eta - \eta_1)} \quad (37)$$

The eigensolution determines λ' and the perturbation amplitude except for an arbitrary constant equivalent to a shift in η . The solution behavior of these three ODEs on the downstream side ($\eta \rightarrow \infty$) satisfying

$$\bar{u} \rightarrow \bar{u}_2 \quad \bar{S} \rightarrow 0 \quad \varphi'' \rightarrow 1$$

is similarly determined as

$$(\bar{u} - \bar{u}_2, \bar{S}, \varphi')^T = (1, B'', C'')^T e^{\lambda''(\eta - \eta_2)} \quad (38)$$

The acceptable solutions must have positive real values for λ' and negative real values for λ'' . The values for λ' and λ'' were computed for the entire range of $M_1 > 1$ by S. Shao in collaboration with the PI. The results are presented in Figs. 6a, b where the acceptable solutions are shown in solid curves. Thus, unlike Grad's 13-moment based system, the boundary conditions at both ends $\eta \rightarrow \pm\infty$ can be satisfied for all M_1 . The single solid curve in Fig. 5 suggests an upstream behavior comparable to a saddle point and, with (37) and (31) or (32) a (unique) solution may accordingly be determined by a shooting method marching from upstream.¹

2.3 Computational Studies: PNS and Other Thin-Layer Approximations

Encouraged by the comparison between DSMC calculations and the 13-moment based shock-layer theory, NS and PNS code development are carried out to substantiate the correlation principle and extend the theory. Sizable errors in uncorrected shock-layer solutions due to poor approximation of the outer edge location is one major reason for carrying out *shock-capturing* NS and PNS calculations (which also furnish the proper "shock slips"). The computation programs developed for the PNS equations provide a more versatile framework for testing the adequacy of the shock-layer and thin-layer approximations, and for comparing/examining the Burnett and other models of translational nonequilibrium.

Thin Layer vs. Shock Layer: PNS Equations vs. PNS Calculations

In the following, the notion "shock-layer approximation" is to be distinguished from the "thin-layer approximation" in that the assumption of the presence of a strong shock with a high compression ratio is *not* used in the latter. In developing the PNS equations and its higher-order form for the present study, the thin-layer approximation was used, which therefore allows application also to a shear/mixing layer. We shall also distinguish PNS equations from PNS calculations in that the latter refers to computations applying a space-marching procedure to the parabolized (thin-layer) NS equations, whereas the former means strictly the parabolized NS equations themselves. This distinction is worthwhile, since the PNS calculations cannot describe upstream influence and streamwise flow separation, whereas, solving it as a time-dependent or iterative problem, the system of PNS equations can recover these missing virtues of the NS equations. The many successful thin-layer codes (e.g. Ref. [33], also refer to review in Ref. [20]) may in fact be considered iterative solution procedures applied to PNS equations, which may or may not include time-dependent terms.

Parabolized PDEs of NS and Continuum Extension

Several versions of parabolized NS, 13-moment and Burnett equations are derived, using *thin-layer* approximations. Marching procedures solving the reduced initial boundary-value problems adopt the Vigneron algorithm [34] in the subsonic layer to suppress departure

¹This work has not been continued since Dr. Sally Shao fell ill late last year. Computation study of the full systems Eqs. (33)–(35) will be resumed with additional help shortly. A research note on the 14-moment analysis has been documented in the proceeding paper [61].

solutions, which calls for the use of a relatively low Vigneron parameter $\omega = 0.2-0.3$ in the 3-D case. In the 3-D version used in the strip-theory validation below, the spanwise convective and diffusive terms are treated *explicitly*, and the remaining difference equations are solved *implicitly* in a *fully coupled* manner, using the Crank-Nicholson type procedure. Shock-capture PNS solvers have been programed for both Cartesian and Dorodnitsyn variables. The solver in the latter variable set can be used to correlate/predict shock-layer flows in translational nonequilibrium via the reduced constitutive relations of the 13-moment theory of Sec. 4.1; it also avoids the difficulty with the shock structure in a formulation in which the 13-moment equations are explicitly solved. (Of course, the PNS solution in other variable sets may still be correlated meaningfully with DSMC and other nonequilibrium calculations when expressed in the Dorodnitsyn or von Mises variables.) The thin-layer equations and their transformation to the computation domain have also been developed to facilitate immediate computational studies for 3-D curved surface and for an unsteady extension. Stimulated by the concurrent time-accurate computational study to be discussed in Sec. 4.4, a code development is underway to adapt an *iterative* procedure used in our earlier work [35] to restore the upstream-influence capability to the PNS equations, which has proved effective in solving the triple-deck viscous interaction problem. These algorithmic developments have been carried out principally by Dr. C. J. Lee and are to be detailed in works to be submitted for publication later.

Improved Correlation with DSMC

As anticipated from earlier studies, the shock-capturing capability of the PNS calculations can substantially enhance the solution accuracy over the FVSL solutions and may improve the agreement with the DSMC calculations through the correlation principle. The case of a flat plate at 40° attack angle in a flow of $M_\infty = 26.8$ in the range of $\bar{x} = 10^{-1}$ through 10 [cf. Eq. [2.2] for definition of \bar{x}] has been used as a generic example comparable to the Space Shuttle descent environment in the studies of Refs. [10]–[15]. Figure 7 presents five data sets of surface distribution of heat-transfer rate from the PNS calculations, correlated and compared with two sets of DSMC calculations (in plus and cross symbols) in terms of the hypersonic rarefaction parameter \bar{x} . Also included is the FVSL calculation from Ref. [9]. Note that the PNS calculation assumes $\gamma = 1.40$ and $Pr = 0.72$, while the DSMC calculations from Refs. [36,37] allowed vibrational nonequilibrium, which is not believed to be important in these speed and rarefaction ranges. The agreement is good, except for the DSMC data set for the 100 km altitude (in crosses). The results of comparison in the skin-friction distributions (not shown) are similar, with the DSMC data set for the 100 km case being again an exception. This is to be more carefully examined in future analyses especially with regards to the upper far boundary location. This form of correlation also succeeds in demonstrating the power of reference-temperature method underlying the use of the parameter/variable \bar{x} , which allows the correlation of gas flows with arbitrary force law with that of a Maxwell gas.

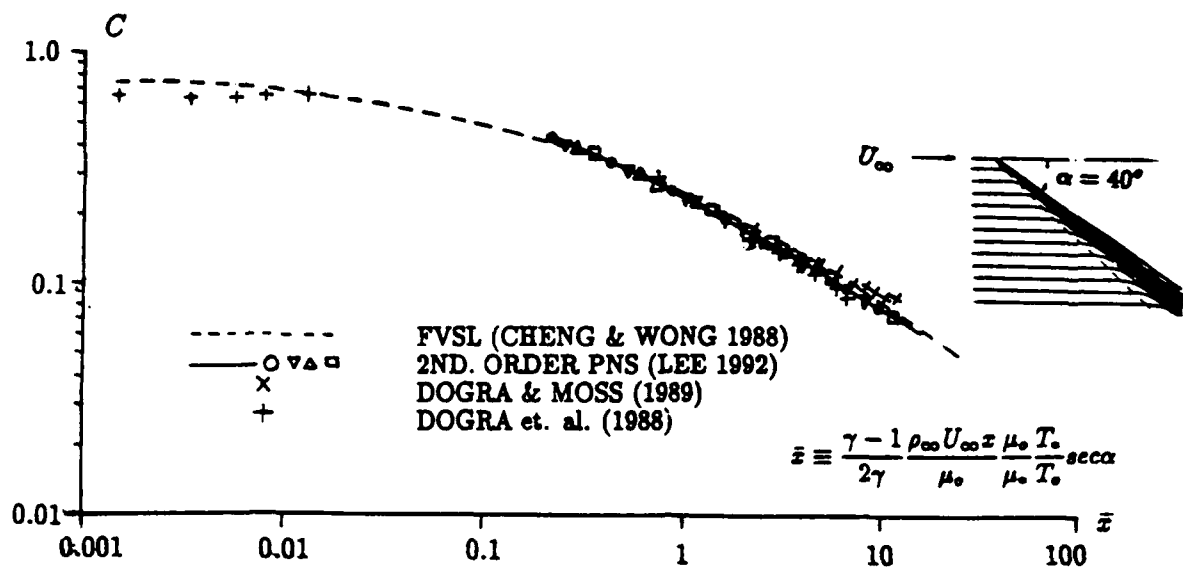


Fig. 7

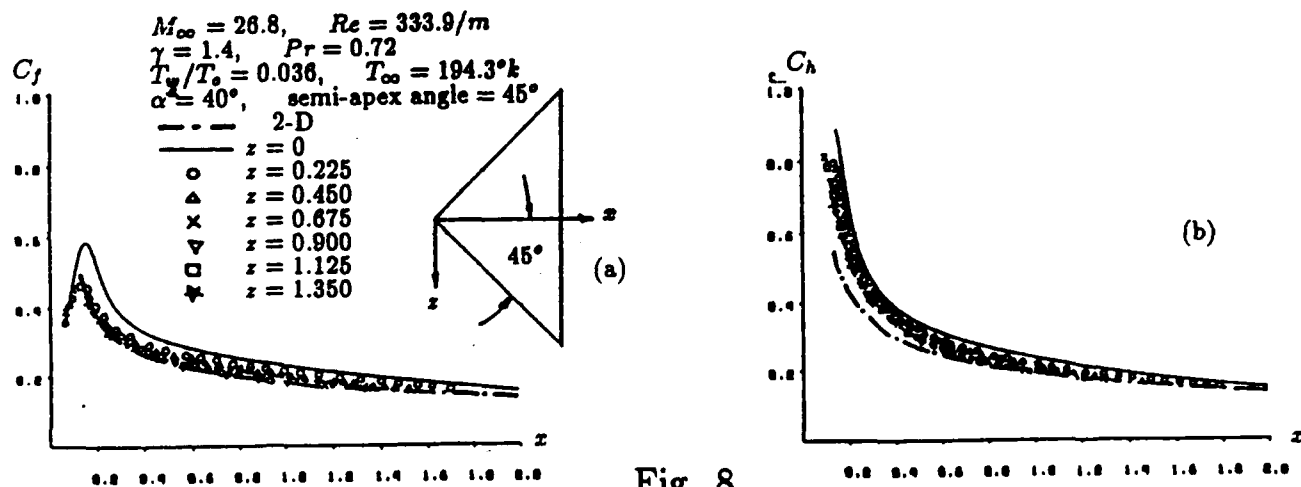


Fig. 8

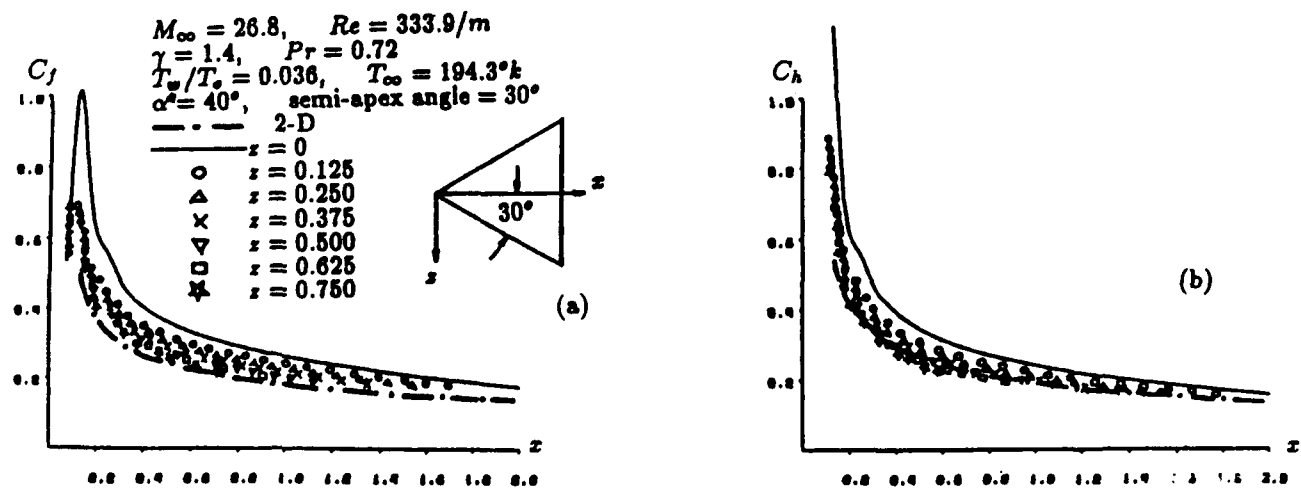


Fig. 9

3-D PNS Applied to Plane Delta Wings: Strip-Method Validation

For a flat surface at incidence, the theory admits a version of the strip method as a 3-D solution to the FVSL problem. As a test of the 3-D formulation, we compare two sets of 3-D PNS calculations for flat wings with 2-D PNS results in accordance with the strip method. Delta-shape planforms with two different semi-apex angles (45° and 30°) were considered. The plate representing the windward flat surface is set at 40° attack angle in a uniform flow with $M_\infty = 26.8$ and a free-stream Reynolds number $Re = 3440$ at the trailing edge in the symmetry plane, where $\bar{x} \approx 3$, for a speed 7.5 km/sec and an altitude 100 km. A model of calorically perfect gas with $\gamma = 1.4$ and $Pr = 0.72$ again suffice.

The surface distributions of 3-D PNS data on skin-friction and heat-transfer coefficients on a number of span stations are presented in Figs. 8a, b for the 45° delta planform and in Figs. 9a, b for the narrower 30° delta surface. The C_f and C_H are correlated as functions of the distance from the leading edge $x' = x - x_{LE}$, in accordance with the strip theory. Excepting data along the centerline (in thin solid curve), the skin-friction data in Fig. 8a correlate themselves very well; the correlation improves with distance from the center line and approaches closely the 2-D solution (in dash-dot curve). The corresponding results for the heat-transfer coefficient in Fig. 8b are similar and the noticeable discrepancy with the 2-D data may well result from the lack of adequate treatment of the leading edge region for the 2-D analysis made earlier. For the narrower delta planform examined in Figs. 9a, b, the discrepancy from the strip theory (the dash-dot 2-D curve) along the center line and the neighboring span stations is noticeable; good agreement among the more outboard span stations are still found, and C_f and C_H data from all span station ($z \neq 0$) seem to correlate surprisingly well over a region $0.05 < x < 0.15$ near the leading edge. The converged data in Figs. 9a, b appear to agree better with the 2-D distribution, hence the strip theory, than in Fig. 8a, b.

In passing, we note that several 3-D DSMC calculations appear recently, which provide good examples for testing their correlation with the NS solutions. One of these examples is a narrow delta wing of triangular cross section considered by Celenligil & Moss [38], for which the 3-D FVSL theory of Refs. [12]–[15] may find difficulty with the ridge in the symmetry plane but is ideal for the 3-D PNS calculations, which remains to be carried out. Another problem of fundamental interest involving the *third* spatial dimension is the search for the spanwise 3-D structure of the viscous shock layer over a curved compression surface/ramp, corresponding to the Görtler vortices in the classical boundary-layer theory. Our formulation and code development for the PNS for curved surfaces noted earlier provides the point of departure for this investigation. We shall return to this subject later in Sec. 3.

Other Thin-Layer Hypersonic Viscous Flow Studies

The thin-layer approximation permits application to viscous hypersonic flow other than the thin shock layer in the foregoing discussion. The examples of the hypersonic shear layer and the aligned flat plate considered below and in the next subsection (§2.4) represent rarefied hypersonic flows, for which (high quality) detailed DSMC calculations has yet to be made and the usefulness of the correlation principle of §2.1 has yet to be established. It

is essential to point out that even though a strong bow shock is not required in the thin-layer approximation, the assumption of a sufficiently small $\epsilon \equiv (\gamma - 1)/2\gamma$ is still needed if the greatly simplified 13-moment based constitutive relations (underlying the correlation principle) is to be kept. Its adequacy remains to be examined.

Hypersonic Shear Layer The highly expanded flow on the lee side of an obstacle should be an important consideration in aerothermodynamic design and in determining the upstream influence of the trailing edge on the compression side (cf. §3.4). A unique feature of this lee-side flow is a shear layer which separates the uniform hypersonic stream and a highly rarefied region bounded by the body surface on the lee. In the example, we consider for simplicity an inclined plate of zero thickness with the same surface and freestream conditions as in examples previously considered.

Ideally, a coordinate system may be chosen with the origin at the leading edge and the x -axis aligned with the free stream, with which the thin-layer equations should describe the shear-layer structure well. Shown (as solid curves) in Figs. 10a, b are the density profiles from the PNS calculations, obtained however with the marching x -axis directed along the plate at 20° attack angle. The results nevertheless agree reasonably well with the converged (time-accurate) NS solutions (in filled circles), confirming the adequacy of the thin-layer approximation as well as the relative insensitivity in the choice of the coordinate orientation. The latter may perhaps be explained by the higher accuracy level of the "PNS" equations used here, which is in fact a *second-order* thin-layer approximation to the NS equation. A more severe test is the corresponding comparison made for the 40° attack angle shown in Figs. 11a, b, for which only the profiles at the more upstream station show noticeable differences between the higher-order PNS and NS calculations. Whereas the kinetic-theory base of the low-density region on the lee side is yet to be ascertained, its influence on shear-layer structure represents an interesting issue. The magnitude of stress ratio $|p_{ij}/p|$ inside the shear layer in these examples turns out to be reasonably bounded, therefore a treatment through the thin-layer 13-moment theory is possible, how should the low-density region be treated and matched with the shear layer in this case remains to be studied.

The Aligned Flat Plate For a flat plate at zero incidence, the strong self-induced pressure in a low-density hypersonic flow is well known. The thin shock layer theory is not applicable in this case. Figures 12a,b,c show comparison of the (second-order) PNS calculations (solid curves) and the DSMC calculations [39] (filled circles) in skin friction, heat-transfer rate and the surface (thermodynamic) pressure. Also included are computations based on the (stabilized) Burnett equations [40] (in open circles). A (monatomic) hard-sphere gas flowing over a cold plate of 150 mean-free paths (mfp) at Mach number 12.9 and Reynolds number 3189 was considered. The Knudsen number in this example is therefore $Kn = 0.00404$, very low. Noticeable differences among these three solutions thus occur only over the upper 5% chord, except in Fig. 12c where the departure occurs upstream of 40% chord. As one moves upstream in Figs. 12a,b, the PNS calculations depart from the DSMC data trend at the same location as the Burnett solution does, surprisingly, they remain in agreement well into their zone of breakdown. It is of interest to point out that, according to the principle elucidated in Refs. [10]–[12], the NS-based pressure p is to be correlated with the wall normal

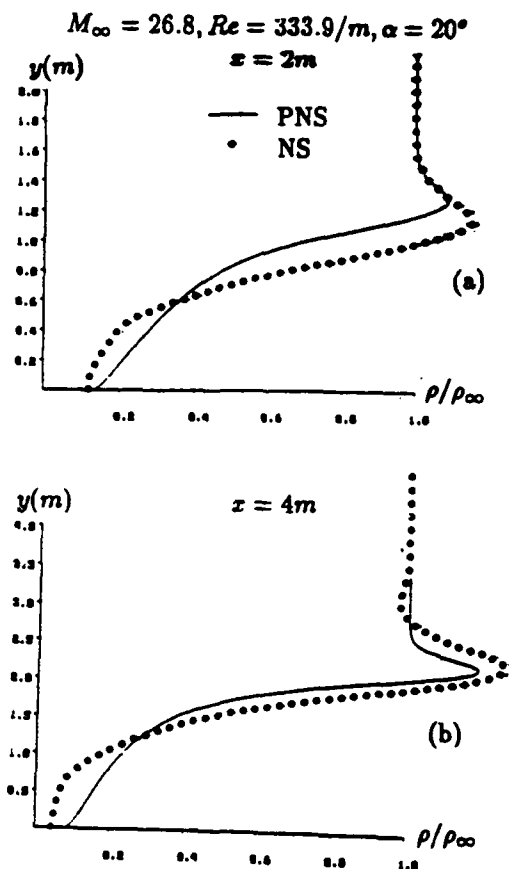


Fig. 10

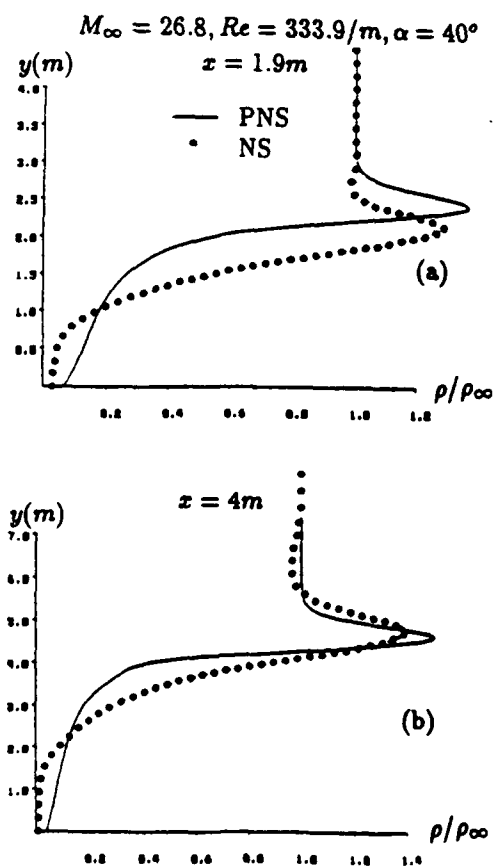


Fig. 11

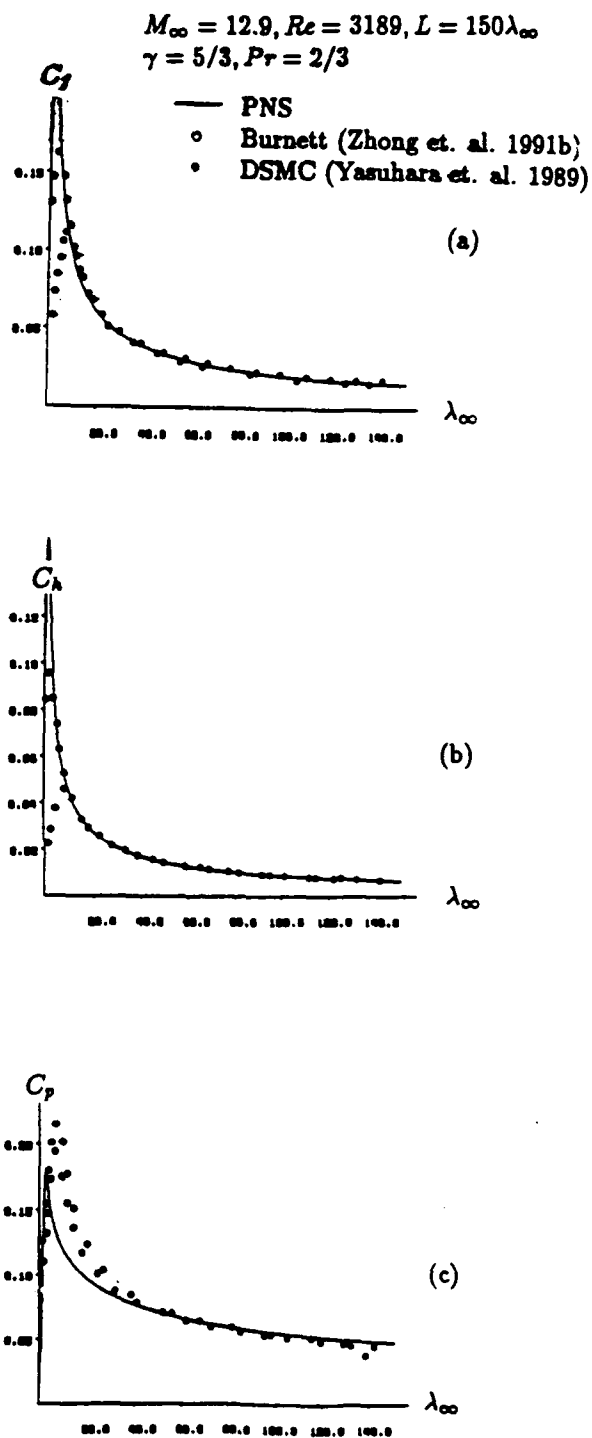


Fig. 12

stress $P_{12} = p + p_{12}$ in the DSMC calculation, therefore Fig. 12c does not offer the correct comparison. Correction would bring the comparison into better agreement, according to the study made for a shock layer [10]–[12]. Zhong et al. compared their Burnett results with DSMC data for blunt obstacles in Ref. [40] where similar conclusions can also be drawn. Thus the Burnett equations do not appear to reduce much of the disagreement between the DSMC and the NS based calculations. The small difference between the Burnett and PNS data in this case may in fact be seen as a result of applying a special solution procedure in Ref. [40] in order to avoid an indeterminacy related to the need of additional boundary conditions [cf. Refs. 19,17].

The Burnett-Solution Indeterminacy A thin-layer or parabolized version of the Burnett equations can be used to investigate whether boundary conditions in addition to those for the NS equations are needed for a unique determination of their solution. Under the thin-layer approximation, a major difference between the Burnett and NS equations appears in the normal stress component p_{22} where derivatives in y higher than $\partial/\partial y$ appears as $\partial^2 p/\partial y^2$ and $\partial^2 T/\partial y^2$, suggesting the need of additional boundary conditions; it amounts to a degree of freedom in describing the Burnett solution if no additional boundary condition were assigned. This anticipation is supported by the nonuniqueness in the solution of a constitutive relation for the p_{22} illustrated below, in which only the $\partial^2 T/\partial y^2$ term of the Burnett system is retained.

The degree of freedom chosen for the following study is the wall shear, i.e., the skin friction coefficient. Figs. 13a shows three examples of the skin-friction distribution to be tested, which are assigned the PNS value upstream of an arbitrarily chosen point, and a constant value downstream of this point. The PNS calculation shown as a solid curve is identical to that in Fig. 12a; Fig. 13b compares the resultant PNS pressure profile (solid curve) with the three sets of model Burnett calculations using the assigned wall-stress values of Fig. 13a, at two stations $x = 60, 150$ mfp. They are seen to be distinctly different from the PNS result (solid curve). A Knudsen-layer like structure is evident and is the result of the extremely low value of Kn (0.0040) adopted from the comparison study in the preceding figures, which could degrade the solution accuracy. A grid refinement study shows however that little is changed in these solutions.

The issue raised in this study led to a more critical examination of the Burnett equations for the steady, *Couette-flow* problem, which can be reduced to an ODE system. Their difference from the NS equations in this case appears only in the normal momentum equation with the appearance of $d^2 p/dy^2$ and $d^2 T/dy^2$. Examination reveals that in addition to the five (boundary) conditions for the NS system, *two* more boundary conditions are needed to fully determine all the constants of integration. These two degrees of freedom may be conveniently taken to be the two pressure walls.

In a recent study, Lee [16] obtained accurate Burnett solutions in four cases with $Kn = 0.01, 0.10$ and 1.0 ; the results for $Kn = 0.10$ with wall slips are shown in Figs. 14a, b, c along with the NS solution (in solid curve). Lee assumes flow symmetry in y and there is therefore only one degree of freedom left. The normalized pressure P is unity everywhere in the NS solution; for the four Burnett solutions, one (...) is computed with the normalized wall pressure $P_b = 1$, one (- · -) with $P_b = 0.90$, and one (- · · -) with $P_b = 1.10$. For the

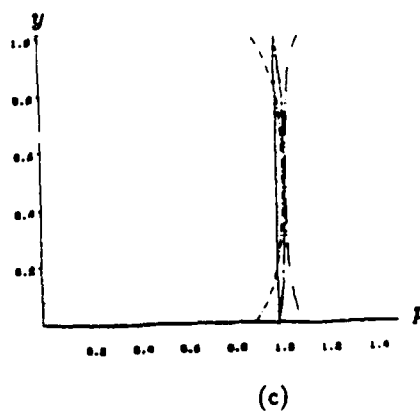
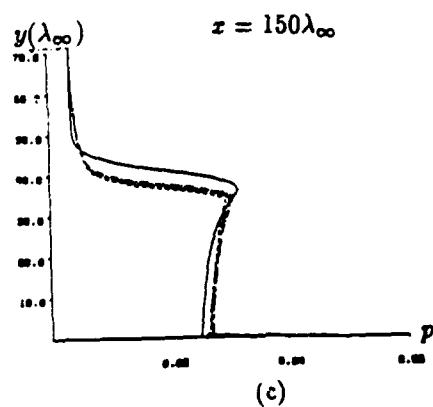
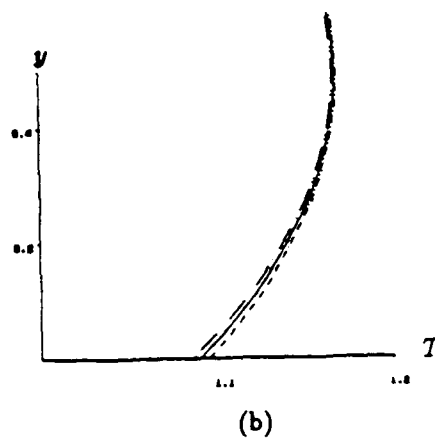
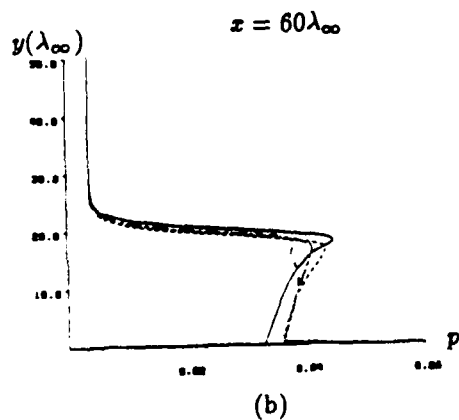
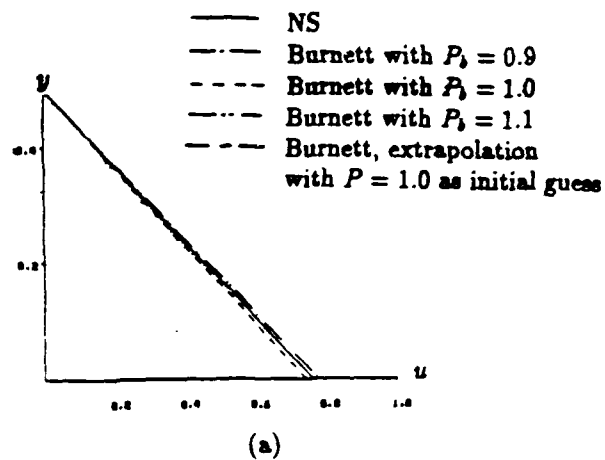
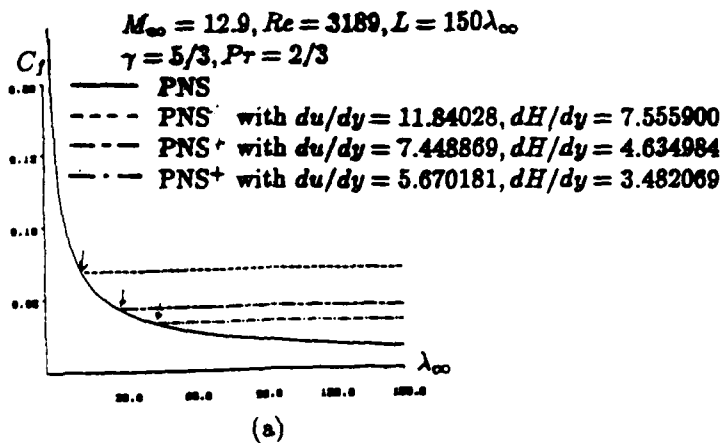


Fig. 13

Fig. 14

remaining Burnett solution (---), the P_b is not assigned but an extrapolation procedure similar to that in Ref. [34] is used next to the wall (using the NS pressure $P \equiv 1$ as an initial guess). The well converged iterative solutions in Figs. 14a,b,c, reveal that Burnett solutions with $P_b \neq 1$ are distinctly different from the others, and that the Burnett solutions using $P_b = 1.0$ and by extrapolation method agree and are indistinguishable from the NS profile in velocity (Fig. 14a) and temperature (Fig. 14b). This study confirm unambiguously the lack of uniqueness in the solution to the Burnett equations without additional boundary conditions. The study also indicates that iterative solution by extrapolation without enforcing the additional boundary condition will converge to the Burnett solution with assigned values of P_b , provided the initial (trial) data satisfies $P = P_b$ at the wall.

2.4 Time-Accurate NS Calculations

The inadequacy of PNS calculations in providing upstream influence is remedied by the (time-dependent or iterative) NS calculations, or their thin-layer versions. Time-accurate compressible NS solvers were used along with PNS codes to lend support to the FVSL analysis and to validate the correlation principle of §2.1. Both explicit and implicate versions of MacCormack's [42,43] predictor-corrector methods have been programmed by Y. Bao and validated earlier with existing computational and experimental data for the compression-ramp problem [43,44] and with DSMC calculations for a flat plate at incidence [12,15]. It was through these time-accurate NS calculations that we recognized the need for correcting the tangential velocity profile in the FVSL analysis and can now explain more satisfactorily the noticeable discrepancy in skin friction and surface-heating rate between the DSMC and PNS or FVSL calculations. The explicit version in rudimentary form has been used for most studies in the present program, which can be considered robust, but proves to be costly in problems involving regions of extremely low density which calls for an excessively small time steps (see below). MacCormack's implicit predictor-corrector procedure may be stable as long as the quotient such as $\nu \Delta t / (\Delta y)^2$ remains bounded, which is in fact as restrictive as a conditionally stable explicit method. Y. Bao's work will be documented along with a more recent study by C. J. Lee using an unsteady procedure based on a thin-layer formulation, in a report [45]. The following describes the few key features in the computation procedure used, some representative results and the highlight of the more recent works which reveal a number of unfamiliar aerodynamic properties in a global viscous interaction and their unique evolution processes.

An Explicit Predictor-Corrector Procedure

The predictor-corrector procedure of MacCormack is applied to the NS equations in finite volume form for a calorically perfect gas. An important method improvement for hypersonic applications here is the implementation of a wall boundary condition concerning the normal momentum flux, which was satisfied formally to a second-order accuracy but proves to be inadequate for the very high wall density under a strong wall cooling. Data smoothing commonly needed in these procedures has been found unnecessary in the Mach-Reynolds number domain considered. For the study of a flat plate at incidence with flap, to which most

of our current efforts were focused, the type of simple grid system illustrated in Fig. 15 will suffice (while more general grid for airfoil study at low Mach numbers has been implemented by Bao et al. [46]). For application to problem with a moving flap, the time-dependence is accounted for in the Jacobian of the grid transformation, which become necessary since the deviatorial stress and heat-flux terms were computed in a transformed computation domain.

A central-difference algorithm for computing flux gradients across grid lines (in the computation domain) was universally used in Bao's program, which is applied also at the grid lines through the flap's hinge and at some distance downstream of the trailing edge (cf. Fig. 15). The latter are, in fact, the *zonal boundary* separating zones of dissimilar grids. The treatment could have been improved through matching the extrapolated gradient values from the two neighboring volume/elements. A careful analysis shows however that the truncation error at the zonal boundary resulting from the simplistic (universal) treatment is surprisingly small, being comparable to

$$\frac{1}{8}\theta^3$$

where θ is the local deflection angle of the grid. The errors amount to a half percent for $\theta_1 = 20^\circ$, and to 4% for $\theta_1 = 40^\circ$. We considered therefore the algorithm to be adequate.

We note in passing that time-split versions of the explicit predictor-corrector procedure as implemented in Refs. [37,38] may reduce substantially the computer-resource requirement. Further speed-up is possible with the explicit scheme (cf. discussion in Section 3).

Aligned vs. Nonaligned Flat Plates

Apart from providing NS data for comparison with the DSMC solution and assessment of the FVSL and PNS calculations, considerable insight on the upstream influence of the flows of interest was gained from the full NS solutions. In particular, the upstream influence of a trailing-edge or corner is much stronger on an inclined plate at large angle, say $\alpha = 40^\circ - 45^\circ$ than on an aligned flat plate or a plate at glancing incidence. This is because a good part of the flow behind the shock is in the low supersonic or *transonic* regime for a plate at large incidence. This explains why a flap/aileron deflection can strongly alter the windward pressure level while little pressure change can be found on an aligned flat plate upstream of a ramp/corner; we shall return to these trailing-edge/flap/corner effects with concrete examples later. In our earlier correlation study for the 40° inclined plates, we noticed a small but distinct feature in the skin-friction and in surface heat-transfer distributions in the case of a monatomic gas ($\gamma = 5/3$). Namely, the skin-friction value tends to flatten out instead of decreasing in a monotone manner towards the trailing edge. Whereas, this feature is not so pronounced for a diatomic gas ($\gamma = 7/5$). The difference may again be explained by the difference in the averaged Mach number in the shock layer. In fact, if not for the wall-cooling effect in the viscous shock layer in these examples, the shock would have detached from the apex for a monatomic gas. Figures 16a, b show for a flat plate at $\alpha = 40^\circ$, $M_\infty = 24.6$, $Re_\infty = 169$ the skin-friction and surface-heating coefficients as functions of the distance from the leading edge. NS data obtained from Bao's program (in open squares) are seen to depart from PNS calculations (in solid curve) and flatten out toward the trailing edge over

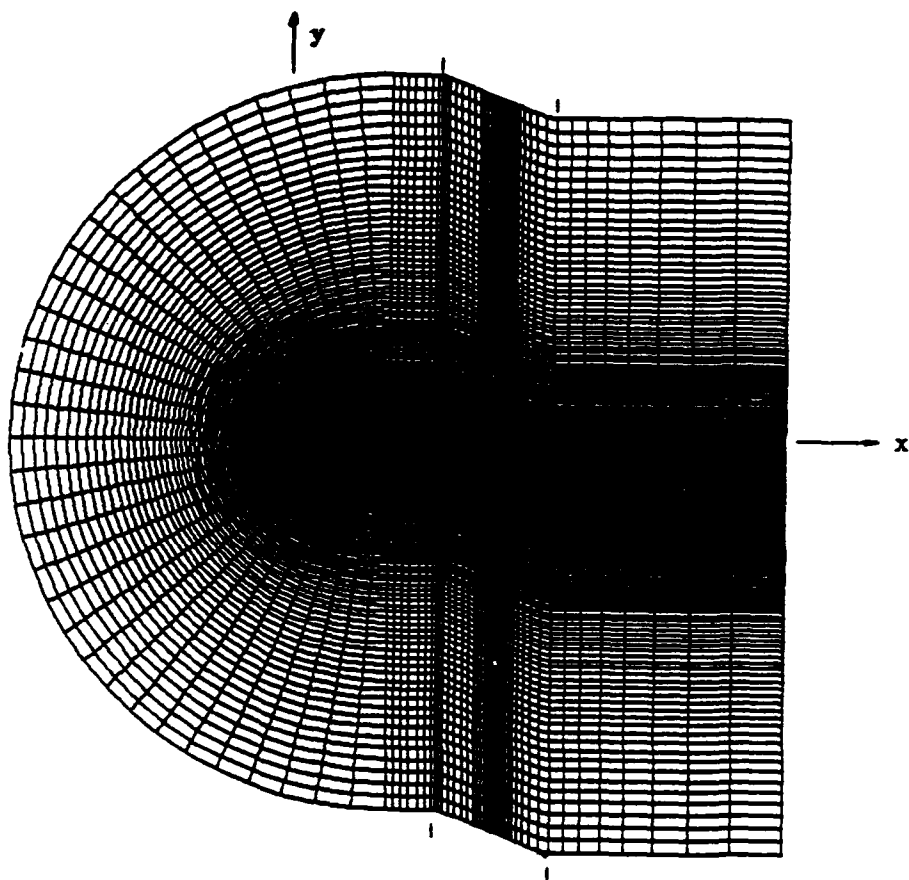


Fig. 15

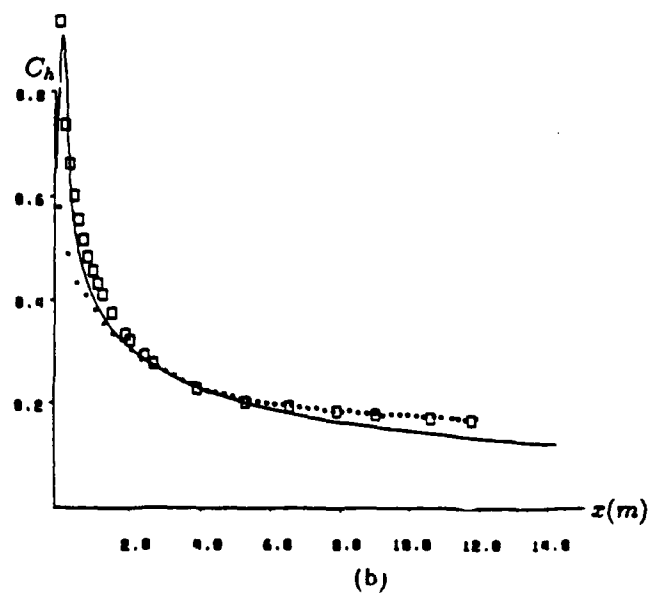
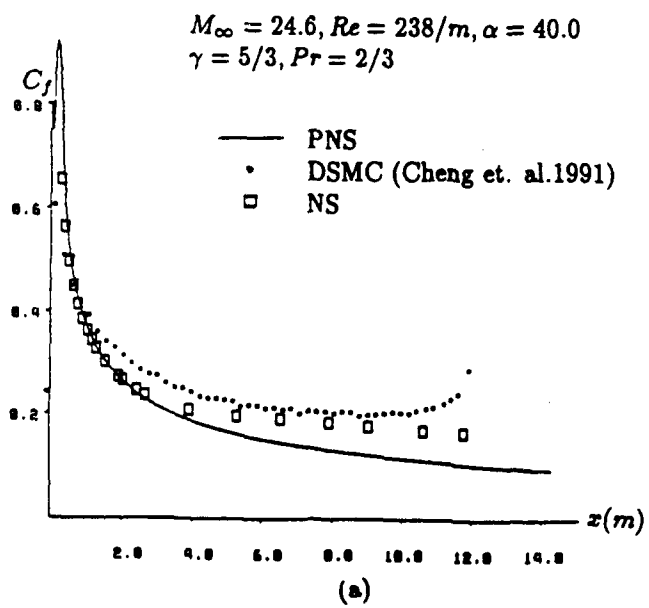


Fig. 16

an extensive range ($x > 3$ m). This trend of the NS data appear to be borne out by the DSMC calculations.

Another difference in flow behavior between the windward flow and the flow on the leeside is in their evolution time (after an impulsive start). The steady-state windward flow field is built up slowly, with a characteristic time many folds the flow-transit or convective time L/U_∞ , owing to the slow upwind propagation velocity

$$L/|a - |u||$$

whereas, the leeside flow can build up quickly, with a characteristic time

$$L/(a + u) \sim L/U_\infty,$$

(see below).

Hypersonic Shear-Layer Evolution

An interesting extension of the thin-layer study is one addressing a hypersonic free shear-layer; the flow on the expansion side of a wedge or inclined plate is one such example. The existence of a distinct shear-layer structure may be demonstrated by the NS solution which evolved in an impulsively started flow. Several sets of unsteady NS calculations have been obtained for the flow on top (and bottom) of flat plates at incidence. Figure 17a shows the density contours above the 40° inclined plane at a time corresponding to $Ut/c \approx 0.81$ after the impulsive start to reach $M_\infty = 26.8$ and $Re = 3340$. This flow-field pattern, together with results at other times, reveal a progressive development and merging of two major regional patterns on the lee side: one represents a Rayleigh-like wave propagation in the direction normal to the plate over the region where the signals from the leading edge have not yet been felt, and the other represents the growth and extension of a shear layer which separates the free stream from a Stoke-flow like, low-density region. The shear-layer structure reaches a steady state readily while lengthens steadily and eventually covers the entire region above the top of the plate; the time required to establish a shear-layer structure at a distance x from the leading edge is comparable to x/U_∞ . Figure 17b shows the computed density profiles for the station $x/c = 0.19$ at three successive times $Ut/c = 0.623, 0.71$ and 0.81 . They are indistinguishable from one another, indicating unambiguously the rapid build up of a steady-state structure for the shear-layer layer on a time scale of x/U_∞ . This example assumes a cold wall and wall slips with unit-order accommodation coefficients; limited differences are found in solution obtained for a non-slip wall.

Flap Deflection and Effectiveness

Flap effectiveness in hypersonic viscous flow has never been critically studied theoretically and experimentally but is an important recent issue affecting the NASP aerodynamic design. Several different groups at NASA Ames and Langley Research Centers and at Alvin Calspan have investigated the various reasons, including nonequilibrium gas dynamics effects, for the failure of earlier analysis in predicting the proper trim angle during the shuttle descent.

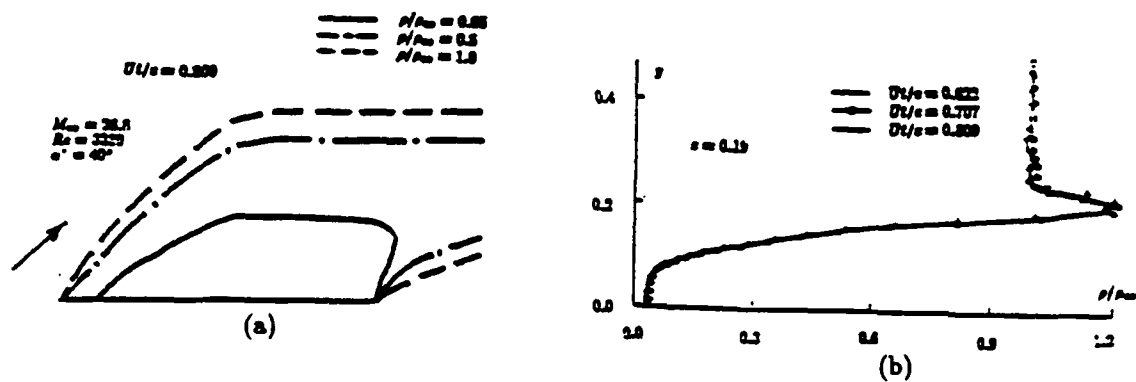


Fig. 17

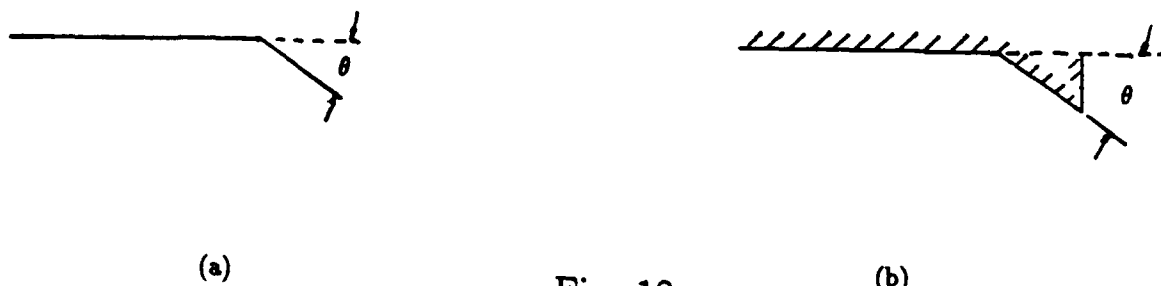


Fig. 18

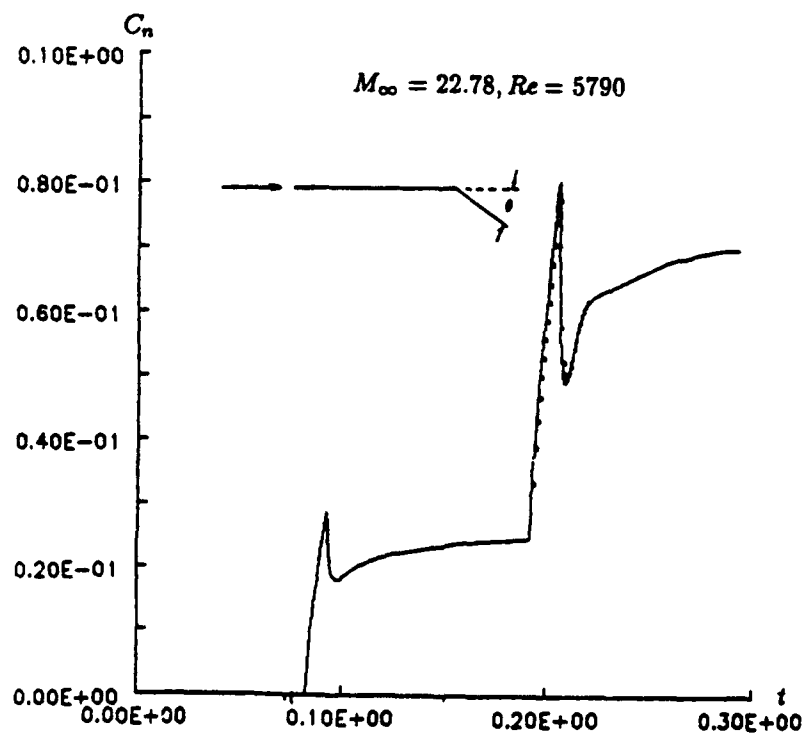


Fig. 19

Gas Model and Geometry As in the nonaligned flat plate studies discussed earlier, the computational study below stipulating a very fast translation-rotation energy transfer in the flow regime under study, therefore a calorically perfect gas with $\gamma = 7/5$, $Pr = 0.72$ is again assumed. A viscosity-temperature law $\mu \propto T^\omega$ with $\omega = 3/4$ is chosen which is believed not far from that used to calibrate the variable-hard-sphere collision model in the DSMC calculations of Refs. [36–38]. The flaps hinge (line) is set at 71% chord ($x_0 = .71$). During the period T^* of an unsteady flap movement beginning at $t = t_0$ the instantaneous flap deflection angle θ_{int} (in radian) is assumed to be given by a *uniform angular velocity* (in radian per sec)

$$\theta_{int} = \omega^* t' \equiv \omega^* (t^* - t_0^*) \quad (39)$$

where t' and t^* are in physical unit. The (new, oblique) coordinates aligned with the flap (x', y') are related to the original, plate-aligned (x, y) coordinated

$$x' = x_0 + (x - x_0) \cos(\omega t'), \quad y' = (x - x_0) \sin(\omega t'). \quad (40)$$

The period T^* is then determined by the maximum deflection angle θ , $T^* = \theta/\omega^*$. Bao took

$$\omega^* = \frac{U_\infty}{L}$$

Hence the flap-activation period in the following examples is

$$T^* = \theta L / U_\infty \quad (41)$$

which is generally a small fraction of the flow transit time. This mode of flap motion thus simulates an impulsive-start motion while avoiding unbounded flow quantities, from which much of the transit flow response can be studied. It is essential to point out that the time interval characterizing flow response below is considerably longer than $\theta L/U$ indicated above, being comparable to 10^{-2} sec. (One half second is believed to be the limit of response time for manual control).

Boundary Conditions As for the examples with zero flap deflection, the origin $x = y = 0$ is set at the leading edge, the uniform flow conditions are prescribed over the upper, lower and the upstream boundaries $y = 1.6$, -1.6 and $x = -1.13$, respectively, and the zero gradient is applied to each flux variables at the downstream boundary $x = 2.14$. A (x, y) mesh of (126×85) grid points were employed in most calculations, using a normalized time step $\Delta t = 2.5 \times 10^{-7}$ in the most demanding case. Impermeable, slip wall conditions are assumed on the plate and flap surface.

The cases analyzed fall in two groups. In the first group, the basic geometry with an undeflected flap is an aligned flat plate, i.e. $\alpha = 0$; its flap deflection θ was chosen originally so that a comparison with available DSMC calculations for a compression *ramp* [42] can be meaningfully made, even though the lack of similarity on the leeside may erode the comparison regarding the upstream influence at large deflection (see Fig. 18).

The second group focus on a more meaningful aerodynamic study in which flap effectiveness on a nonaligned plate at $\alpha = 40^\circ$ were investigated.

Flap on Aligned Plate ($\alpha = 0$) Moss et al.'s DSMC study [47] on aligned flat plates with *ramps* of several deflection angles (cf. Fig. 18b) under free-stream conditions corresponding to four combinations of M_∞ and Re_∞ . The aligned flat plates with *flaps* considered here use the same M_∞ , Re_∞ and the hinge location x_0 . Solution for a finite plate at $\alpha = 0$, with the flap undeflected ($\theta = 0$), is first obtained by an impulsive start at $t = 0$ to reach a uniform free stream condition at $M_\infty = 22.8$, $Re = 5790$. The steady state is closely approached after $t \simeq 0.06$ in this case. (Recall t is normalized by L/a_∞ .) The flap is then set into motion at $t \approx 0.08$ at a uniform angular velocity in the manner of Eq. (39) until the flap angle reaches $\theta = 15^\circ$, and the flap position is frozen thereafter. A steady pressure built up on the compression side of the flap occur during the flap movement, which is followed by rapid pressure drop after the flap stops. A long transient ($0.10 < t < 0.19$) then follows during which the normal-force coefficient rises steadily towards the steady-state value $C_N = 0.024$; the flap is activated again at $t \approx 0.19$ in the same manner as before, increasing θ from 15° to 35° . A flow development rather similar to the previous activation cycle takes place at a higher pressure level with the final and normal-force coefficient to reach $C_N \approx 0.070$ at $t \simeq 0.29$. The normal-force response to these two consecutive flap movements which exhibit the three distinct transients during each activation cycle is shown in Fig. 19.

It is important to ascertain the solution accuracy with respect to the time step Δt . We therefore repeated the calculation of $t = 0.19$ – 0.29 with a time step one half of that used earlier; the evolution history obtained is indistinguishable graphically from that of Fig. 19. The result obtained may therefore be considered *time accurate*. The surface distributions of skin friction, heating rate, and pressure coefficients on the compression side inferred for the steady states from the calculations at $t \simeq 0.19$ and $t \simeq 0.29$ are shown in Figs. 20a,b,c and Figs. 21a,b,c, respectively. Note that the upstream influence of the flap and the trailing edge is not very extensive for $\theta = 15^\circ$, especially for the surface-heating rate C_H in Fig. 21a. Even at the larger flap angle $\theta = 35^\circ$, the region upstream of the mid chord of the *aligned* plate is not at all changed by the deflection. This observation is borne out by the DSMC calculations for the ramp problem [42] of which the corresponding C_f and C_H data (belonging to case I of Ref. 29) are included in Fig. 20 as an open circle. The comparison suggests that the difference between the flap and ramp configurations (Fig. 19a vs. Fig. 19b) is not large enough to be manifested noticeably in C_f but it appears to change the C_H level over the flap.

The abrupt increase of the local C_H level as well as other uncertainties in DSMC solution for this case is exceptional among examples of viscous interaction and require scrutiny. Further comparison between the DSMC and NS data is therefore not made until the DSMC calculations are repeated (using our own code). It is interesting to note that the flow is not yet separated even at a flap angle $\theta = 35^\circ$ for this aligned plate and that the C_f behavior around the hinge is of the type familiar from the triple-deck theory [43]. Figures 22a,b show another set of steady-state results on the aligned plate ($\alpha = 0$) for $\theta = 35^\circ$ for $M_\infty = 24.3$, at a higher Reynolds number $Re_\infty = 12,750$ (corresponding to the Case-2 ramp problem in Ref. [47]). A reverse-flow region does appear over $0.67 < x < 0.80$ in this case (cf. Fig. 22a), but is considerably shorter than that in the corresponding ramp problem by DSMC calculation [47]. This is not surprising since the ramp problem has a base pressure higher

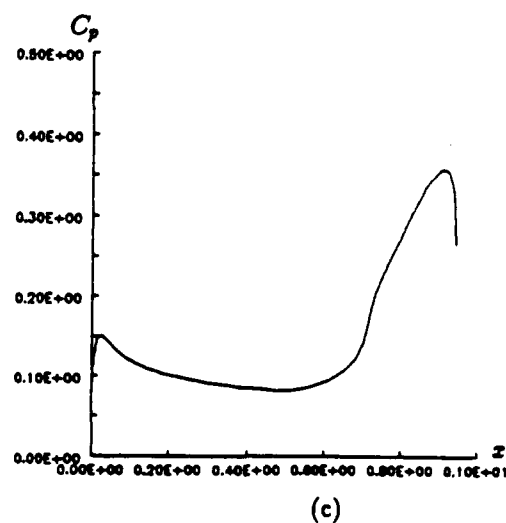
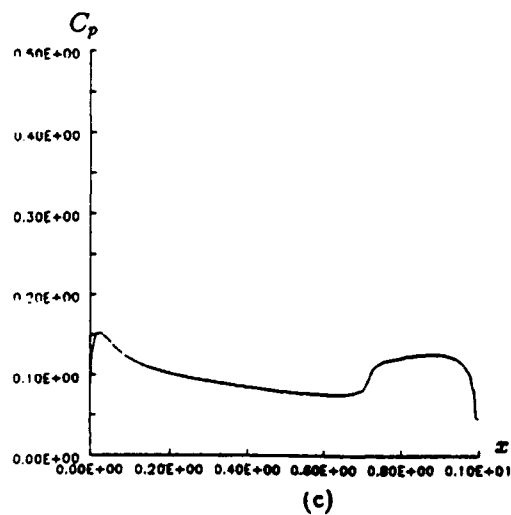
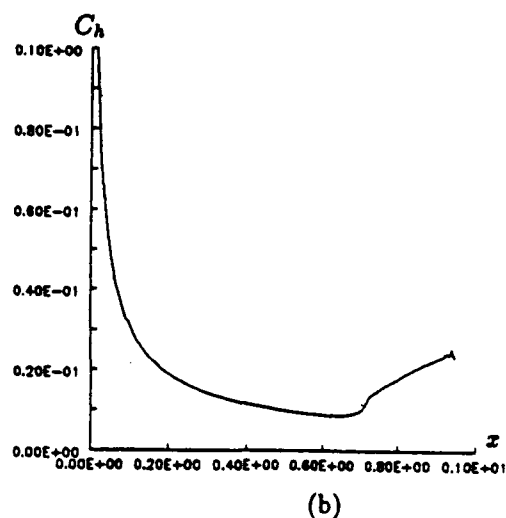
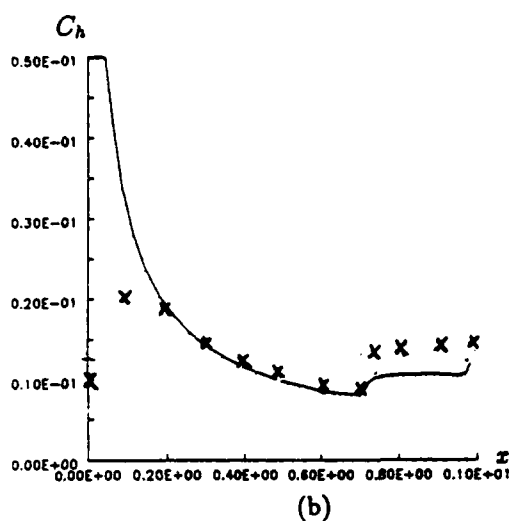
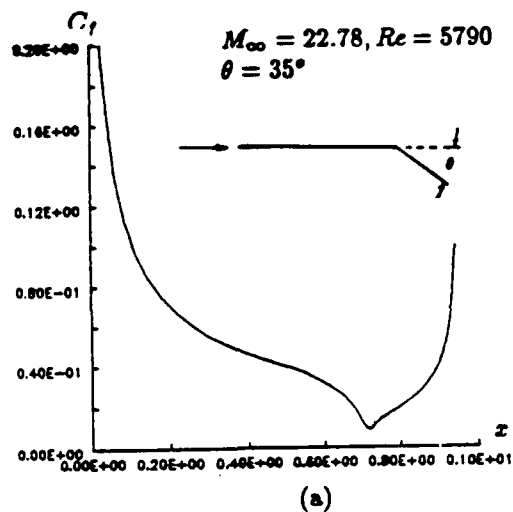
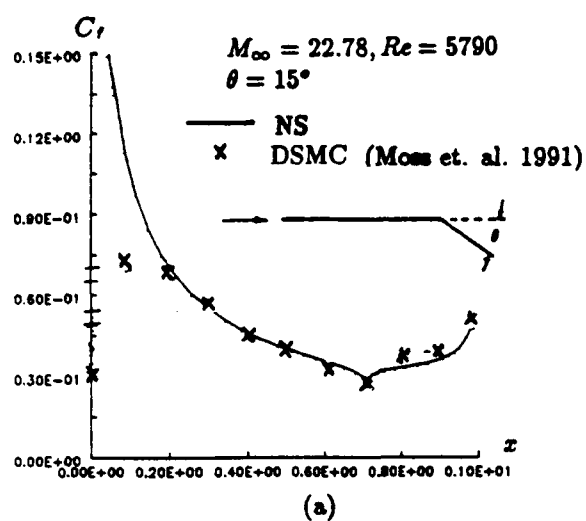


Fig. 20

Fig. 21

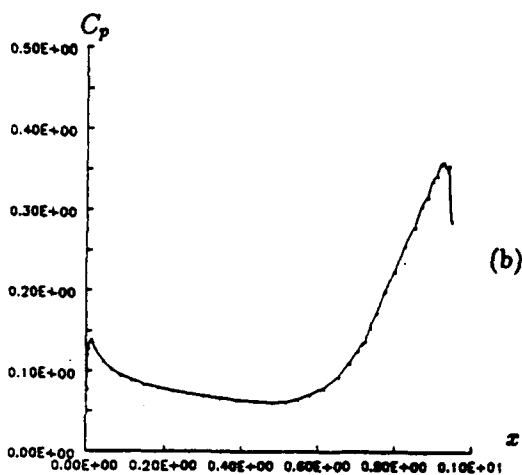
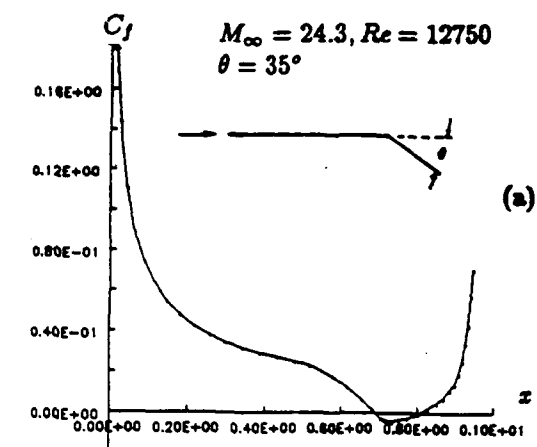


Fig. 22

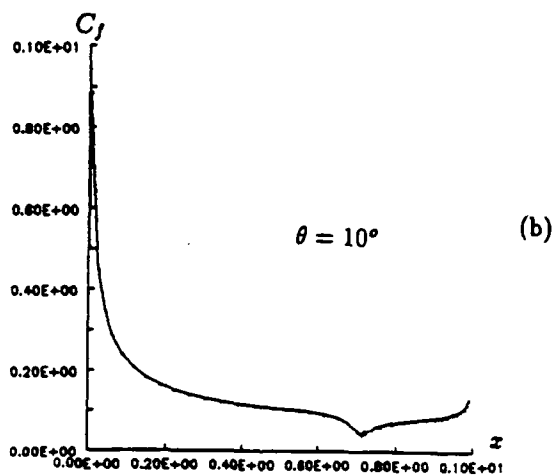
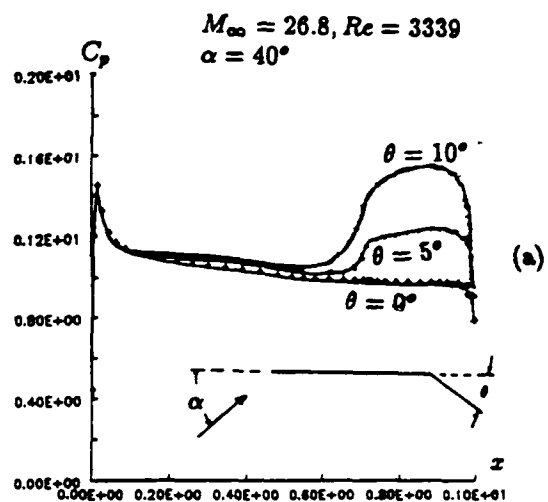


Fig. 24

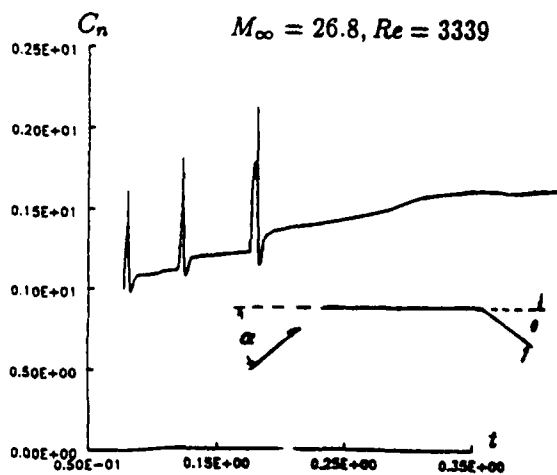


Fig. 23

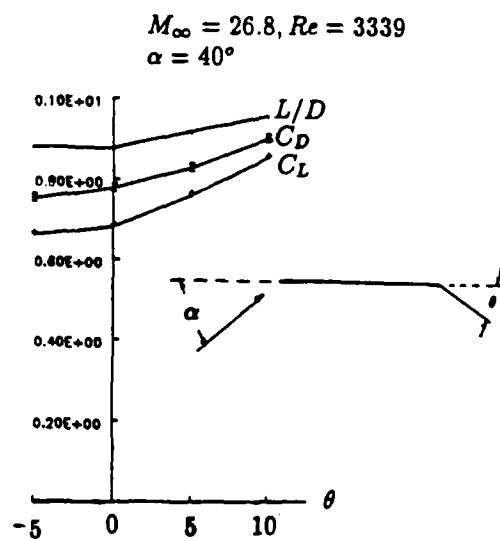


Fig. 25

than that at the flap's trailing edge, hence a higher adverse pressure gradient.

Flaps on Flat Plates at Incidence Flap effectiveness on an aligned plate and on a non-aligned one are very different, especially for plates at high attack angles. The following present examples of nonaligned plates at attack angle $\alpha = 40^\circ$, $M_\infty = 26.8$ and $Re_\infty = 3339$ corresponding to a plate of length $L = 10$ m at speed $U_\alpha = 7.5$ km and altitude 100 km. The wall conditions, the specific-heat ratio, the Prandtl number, and the viscosity-temperature relation are the same as stated earlier. For this study, time-accurate NS solution with flap activation and the aerodynamic response are studied in three consecutive stages: (i) $\theta = 0 \rightarrow 5^\circ$, (ii) $\theta = 5^\circ \rightarrow 10^\circ$, (iii) $\theta = 10^\circ \rightarrow 20^\circ$. The computation is continued for each stage until a steady state is satisfactorily reached before the commencement of the next stage. The flow and aerodynamic response in stage (i) and (ii) are similar to those seen earlier. Figure 23 shows the normal-force development of the consecutive stages. Except for the higher pressure level, the response behavior for the first two stages is similar to that seen earlier from Fig. 19 for the aligned plate (although noticeable upstream influence in pressure is found to be far reaching). The last stage ($\theta = 10^\circ \rightarrow 20^\circ$) turns out to be much longer in the transient, giving rise to unusually high response in normal force and several uncommon dynamical features. The surface distribution of the (steady-state) pressure coefficients (on the compression side) for flap deflected at 5° and 10° , at the end of the first and second stages, are shown in Fig. 24a and compared to the compression side distribution on the flat plate ($\theta = 0$). Here, the weak but noticeable upstream influence on C_p is clearly evident over almost the whole chord upstream of the hinge line even for a deflection as small as 5° . The corresponding skin-friction coefficients are shown in Fig. 24b where the triple-deck type behavior about the hinge line is again seen. Flow separation apparently will not occur until a deflection reaches an angle considerably larger than $\theta = 10^\circ$.

A negatively deflected flap $\theta = -5^\circ$ has also been analyzed for $\alpha = 40^\circ$, for which the upstream effect on surface pressure is found to be far less than in Fig. 24a. The change in normal force and skin friction in this case is such that the decreases in drag and lift (contributed by the windward side) at $\theta = -5^\circ$ is less than the increase at $\theta = 5^\circ$, as shown in Fig 25. An up flap ($\theta = -5^\circ$) is seen to improve the L/D slightly even though much more can be gained with a down flap ($\theta > 0$). At an attack angle not as high as 40° , the flap is less effective. Calculated results for a case identical to those of Fig. 24a, except for a lower attack angle $\alpha = 20^\circ$, confirm that the fractional pressure increase over the flap is less than that in Fig. 24a for $\alpha = 40^\circ$ with much weaker upstream influence.

As may be seen from Figure 23, the normal-force coefficient has a noticeable change in the manner of growth after $t \approx 0.239$. In fact the corresponding change in surface pressure distribution is far more drastic as detailed in Figs. 26a,b for the two successive periods $t = 0.239 - 0.3469$ and $t = 0.3498 - 0.4183$, where the windward C_p -distribution for $\theta = 0$ is also shown in small filled squares. Though not shown, significant pressure build up on the windward side of the flap ceases prior to $t = 0.239$ and large upstream movement of the pressure maximum away from the flap area begins thereafter (cf. Fig. 26a); the sharp peak next to the leading edge is to remain unaffected up to $t = 0.350$. In the following period (cf. Fig. 26b), the nonuniform pressure ahead of the hinge line levels itself out, while the pressure on the flap reduces slightly and uniformly; the sharp peak near the leading edge

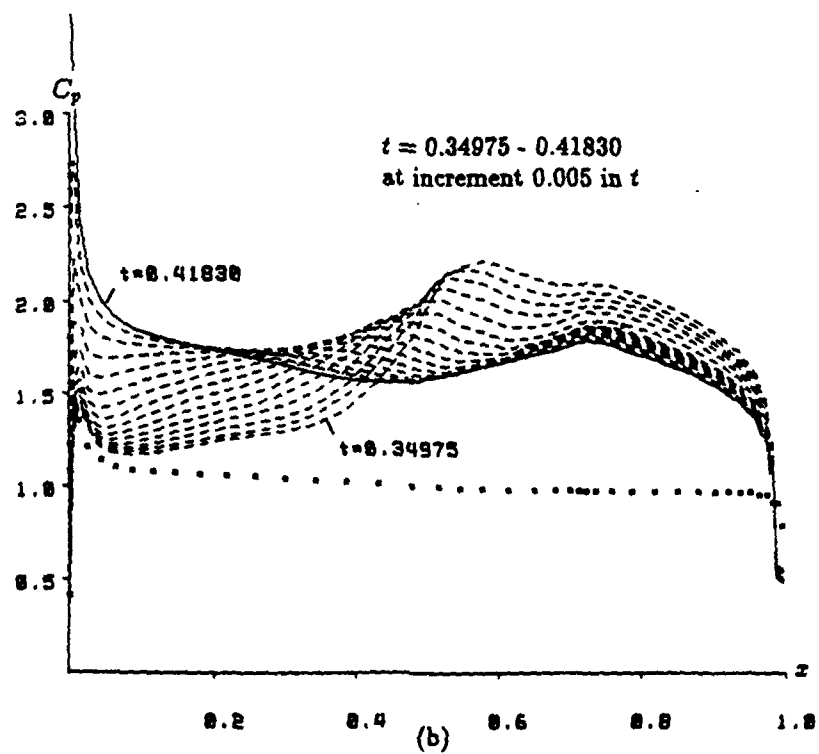
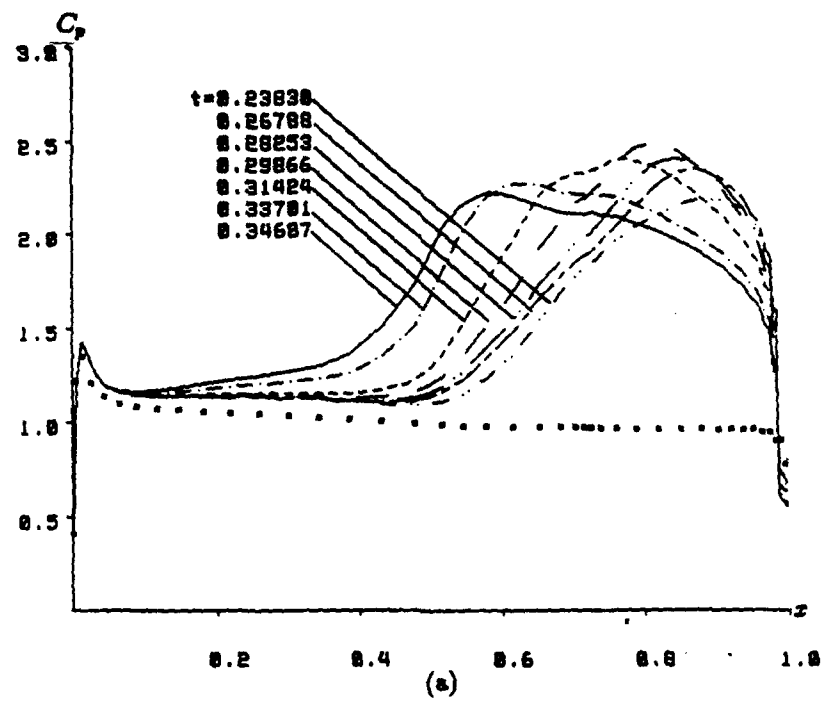


Fig. 26

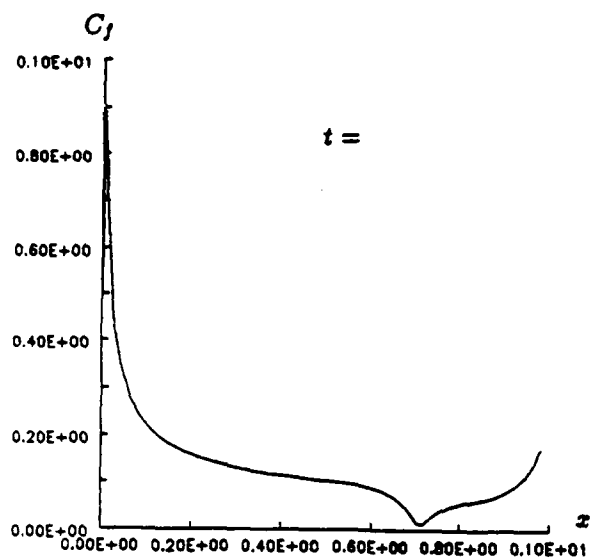
now grows with time.

Interestingly, over the period $t \approx 0.24 - 0.42$, the mean value of C_p , i.e. C_N , changes little from a high 1.7, while the center of pressure shifts from 80% chord to the mid chord. We have yet to complete the calculations for the approach to a steady state, but the final C_N cannot be too far below the present value for reason to make apparent shortly. This value of 1.7 resulting from a 20° flap deflection is far higher than $C_N = 0.51$ estimated according to the Newtonian theory. The increase over the value for an undeflected flap is 62% for $\theta = 20^\circ$ according to the present calculation, compared to only 24% increase according to the Newtonian theory.

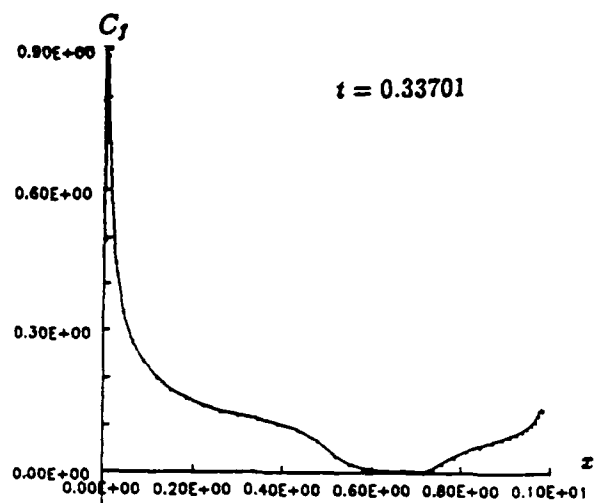
Flow separation does occur during this transient and first appears at a t not far from $t = 0.239$. Figures 27a-e show that the local skin-friction coefficient vanishes shortly before $t = 0.239$ (cf. Fig. 27b) and the reverse flow region spread subsequently over 10% chord length around the hinge line ($x = 0.71$) at $t = 0.314$ (Fig. 27c). The shallow bubble turns into slow-flow region of positive shear shortly after (Figs. 27d,e). The disappearance of the reverse-flow region may be explained by the movement of the pressure maximum from behind the hinge line to a forward position, thereby altering an unfavorable to a favorable pressure gradient.

More revealing is the pattern and change in the velocity-vector field during this period shown in Figs. 28a-f. Two distinct parts of the bow shock can be identified in Fig. 28a ($t = 0.238$) where the part with a higher slope is seen to begin at the x -station shortly downstream of the hinge line (the surface normal drawn from this location would intersect the mid point of the flap). Right behind this shock is a region of exceptionally low velocity. It must be pointed out that this and subsequent pictures represent the continuation of an earlier flow-field development where the stronger, real portion of the bow shock resulting from the flap deflection has not moved as far away from the flap as in this and the subsequent figures. The head of this low speed region surges forward while real part of the bow shock propagates farther away from the flap (cf. Figs. 28a,b,c). Subsequently, the front part of the bow shock join up with the stronger shock and the entire field is engulfed by the enlarged slow-speed region. The evolution pattern shown here is in accord with the surface pressure development (Figs. 26a,b) examined earlier. An interesting property of Figs. 28a-f is in the extreme insensitivity in the flow field in the lee throughout the entire period of change on the windward side, which may provide an opportunity for computer code improvement with zonal strategy.

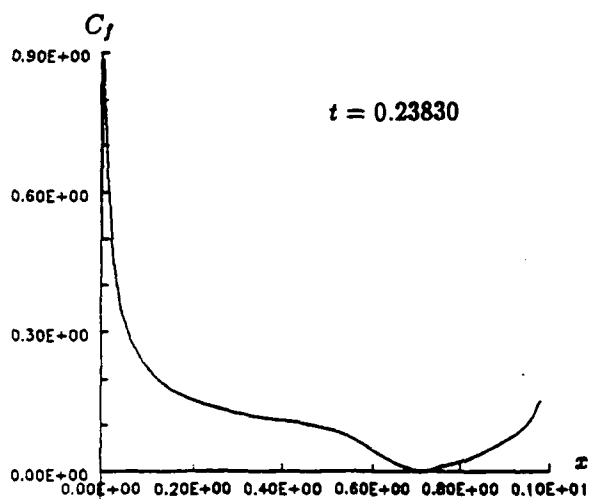
The flow features and behavior observed above are more explicitly brought out by the detailed profiles of velocity, Mach number and other flow variables. Figure 29 gives the profile of the u -component as a function of y on the windward side at the 75% chord station at $t = 0.239$. The minimum velocity in the low-speed region is seen to be a very small fraction of the freestream value and occurs immediately behind the shock indeed. (The u and y of Fig. 29 are those in the original cartesian coordinates aligned with the flat plate therefore is not the tangential velocity profile in a strict sense.) The profile at this station and time indicates also the existence of a high-speed region/layer with a half of the freestream u -value at its peak, which appears to be a necessity at this stage in order to accommodate the mass and momentum fluxes in the shock layer upstream. This profile also implies the existence of



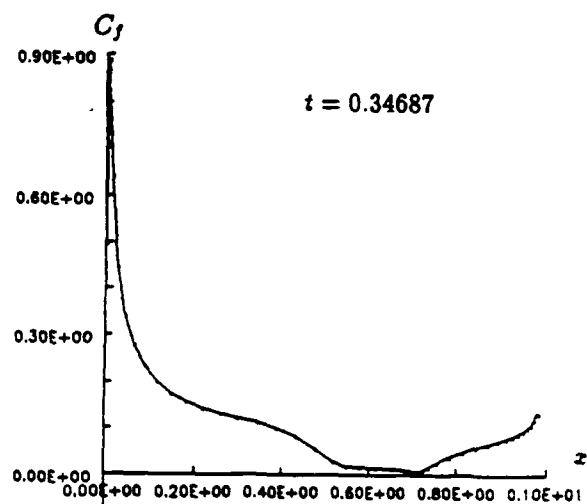
(a)



(d)

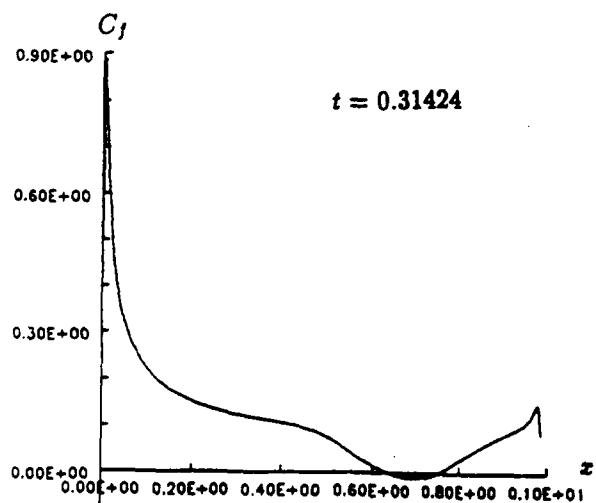


(b)

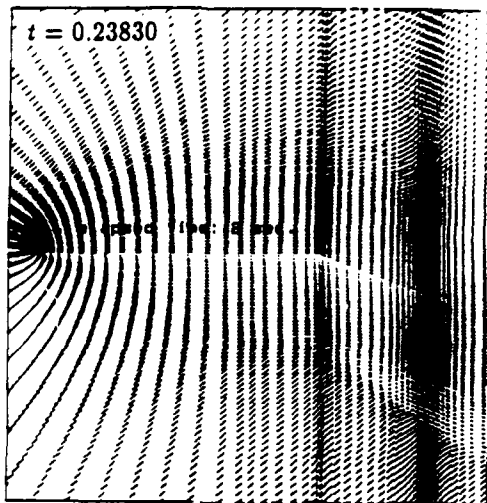


(e)

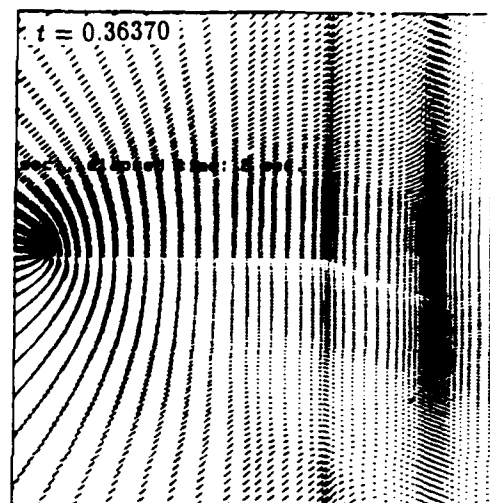
Fig. 27



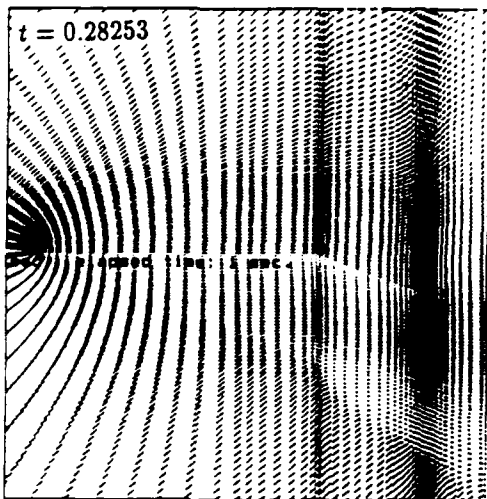
(c)



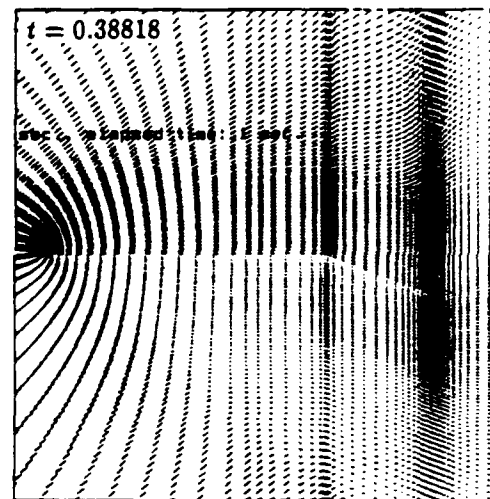
(a)



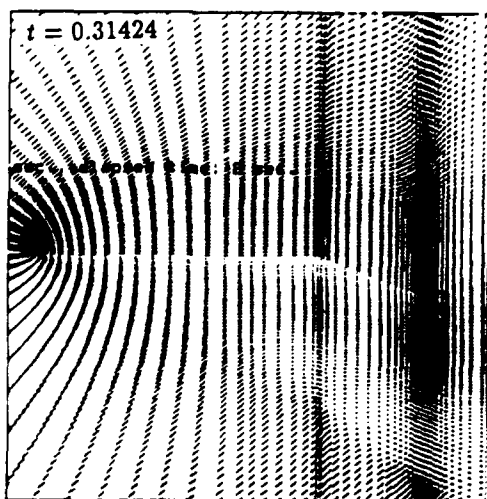
(d)



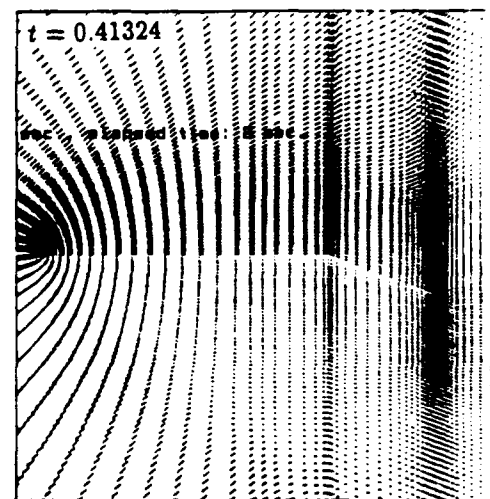
(b)



(e)



(c)



(f)

Fig. 28

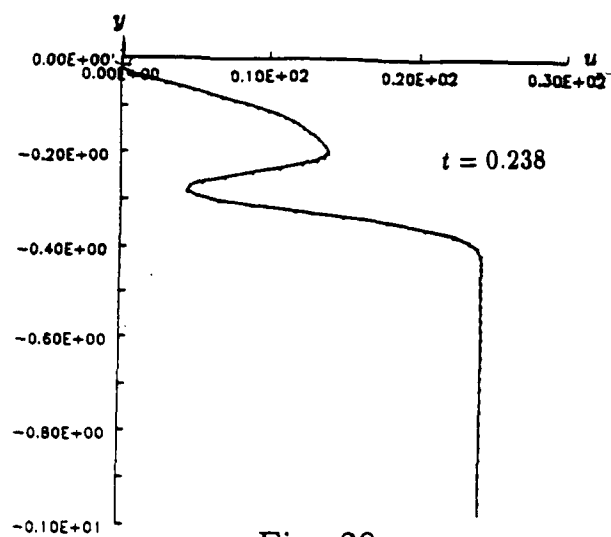


Fig. 29

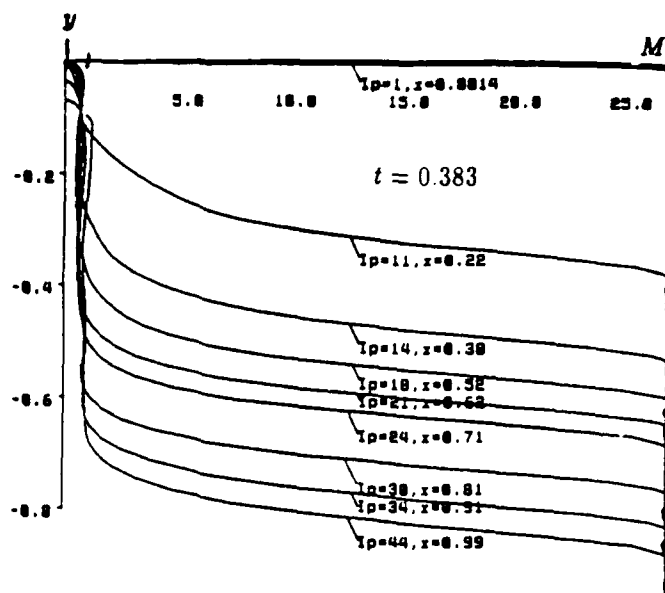
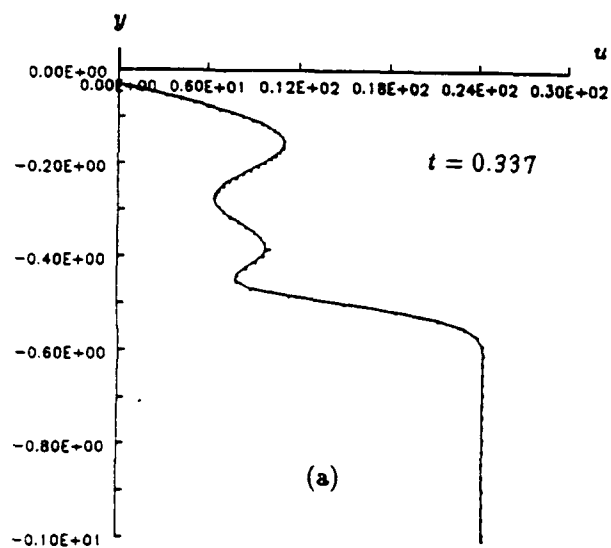
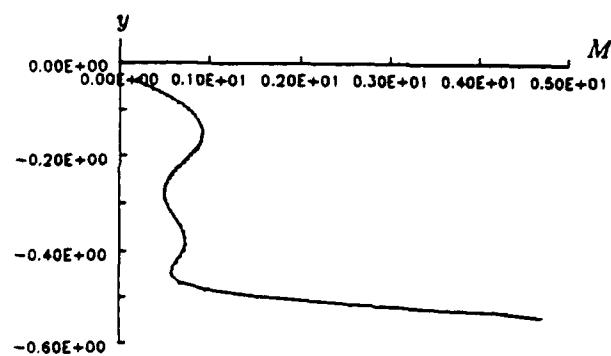


Fig. 31



(a)



(b)

Fig. 30

a shear layer separating the high- and low-speed flows, which may be back traced upstream to the intersection/merging of the two parts of the bow shock. There is a high degree of similarity between the flow patterns related to Figs. 28,29 and an inviscid phenomena of interaction of bow shock and oblique shock—the Edney problem familiar in the supersonic shock and cowl-lip interference problem.[19,44]

Flap Effectiveness at High α as a Viscous Transonic Phenomena The admissibility of the low-speed flow right behind the shock which underlies most features and processes discussed above may have been anticipated from the gas dynamics of an oblique shock, even though viscosity is an important ingredient of the solution. The shock angle β on the stronger, real part of the shock (over the flap) in the present case must exceed 60° by at least 5° – 10° , as indicated by the patterns shown in Figs. 28a–f. Now for a $\gamma = 1.40$ and $M_\infty = 26.8$, the (inviscid) oblique shock relation indicates a Mach number range $0.9 \leq M_2 \leq 1.1$ behind this shock, which also includes the angle at “shock detachment” [49,50]. Large amplitude waves will make the local Mach number even lower. Therefore, the low-speed region may be identified with a property of nonlinear transonic flow, and furnishes a channel for (slow) upstream propagation of (nonlinear) disturbances. This mechanism of upstream influence is unavailable in the aligned-flat case or at low attack angle.

Figure 30a shows another u-profile at a later instant $t = 0.337$ at the station $x = 0.78$ which has two maxima and two minima, and the velocity level becomes higher than in the preceding figure; nevertheless the corresponding Mach number profile in Fig. 30b shows that the entire region between the shock and the flap is subsonic. A more thorough examination of the corresponding Mach number profiles is presented in Fig. 31 for the instant $t = 0.383$ at eight x-stations over the plate. The entire viscous shock layer downstream of the quarter chord becomes transonic and high subsonic in this case. In view of the transonic and subsonic character of the phenomena, an inviscid analysis of the flap effectiveness at a high incidence close to the shock-detachment angle may shed valuable insight into the upstream-influence mechanism for the viscous flow study. To further explore and ascertain the foregoing features of flow behavior, a new time-dependent NS program based on a thin-layer version are being developed and applied to examples of lower Mach and Reynolds number.

3 New and Unresolved Issues

In the foregoing review, important unresolved and new problems are identified. The outstanding one among these are discussed below.

3.1 Gas-Kinetic Based Extension of the Continuum Model

Comparison study of the 13-moment based thin-layer flow model with particle simulation calculations has yet to be carried out much more extensively and in detail to test the “correlation principle” in important cases of rarefied hypersonic flows other than flows on the windward sides of nonaligned flat plates. Improvement in ways of implementing the DSMC calculations, e.g. via parallelism and zonal strategy, may help to increase the productivity of this comparison study.

Gas-kinetic based improved constitutive relations should be derived to be compatible with the corresponding shock-structure analysis (cf. §3.4) and to account for the persistent influence of the upstream state unaccounted for in the present 13-moment based analysis. The study of rotational/vibrational nonequilibrium (cf. §3.5) requires an extension of the thin-layer moment equations to a gas mixture.

3.2 Use and Implementation of PNS Equations; Görtler Vortices and Upstream Influence

Apart from its application to a number of 3-D examples with which the principle for correlation with nonequilibrium DSMC calculations can be examined, the 3-D version of the PNS calculation procedure developed for a curvilinear coordinate systems can be used to study the Görtler vortices on a curved compressive ramp, which has become an important underlying issue in hypersonic boundary layer instability and not treated in the context of viscous shock layer.

A fruitful development which can significantly expand the scope of our current PNS work is to use our *parabolized equations* in an *iterative* procedure, in a manner similar to several existing "thin-layer NS" code for solving *elliptic* problems. An objective in development the iterative procedure here is to reach a steady-state solution cost-effectively for those problems with significant upstream influence. Our iterative version is expected to be more superior than the standard thin-layer code in that initial data can be provided by the marching PNS calculations, apart from the use of a more effective procedure in "delta form" with Newton linearization. The latter procedure has been used successfully in our earlier work on a triple-deck theory of hypersonic viscous interaction [35].

A procedure based on the time-dependent version of the PNS equations will also be considered which will enlarge the parameter domain for the solution convergence/stability and to provide an alternative to the costly predictor-corrector procedure (cf. §3.3) in time-accurate calculations.

3.3 Flap/Aileron Effectiveness: Time-Accurate NS and DSMC Calculations

Our time-accurate NS calculations for flap effectiveness in rarefied hypersonic flows over aligned and nonaligned flat plates have uncovered several unsuspected dynamical features and their evolution processes, which are potentially significant to the hypersonic aerodynamics at very high altitude. The flap/aileron appears be far more effective at high attack angle than commonly realized, and its effectiveness is attributed to the nonlinear transonic flow behavior behind the interacting strong shocks and is believed not tied strictly to the predominant viscous character of the flow. The time-accurate computation discussed at the end of §2.4 has not yet completed to answer the question of whether a steady state can be reached before the shock (structure) *detaches* from the apex. If such a detachment does occur, the transient period to reach steady state would be even longer, making the time-accurate calculation even more important for aerodynamic control application.

More extensive time-accurate NS calculation and method of improving its computation efficiency are essential in reaching concrete and useful conclusions in this study. The 2-

D time-accurate calculations of the flap in §2.4 used 1.5×10^{-5} sec/grid point/time step on CRAY-YMP 8/864; it needs 10 CPU hours to reach a steady state (after an impulsive start). Improvements of Bao's explicit prediction-corrector program are needed in a number of places, with regards to the outer boundary location and conditions, treatment of differencing across the grid's zonal boundaries, the opportunity for effective implementation of zonal and time-splitting strategies. How to obtain/sample meaningful time-dependent data from DSMC calculation represents a new aspect for particle-simulation technique. [Some preliminary study of an unsteady Couette-type problem using DSMC has been initiated at the University by another research group].

Since the underlying flow process and novel features observed here is transonic, nonlinear and vortical in character, the study of flap activation at high attack angle should include examples at higher Reynolds number as well as lower Mach number, than shown above.

3.4 Quasi-1-D Shock Structure

The DSMC study of the quasi-1-D oblique shock structure (with a nonuniform downstream) and a corresponding study by the 14/15-moment or multi-modal approach detailed in §2.2 have made substantial progress and need further work to achieve an adequate flow field analysis, which includes the shock structure, and to provide a basis for improving the gas-kinetic based shock-layer theory.

As noted in §2.2, the 14-moment analysis has succeeded in establishing the upstream and downstream solution behavior which Grad previously failed with his 13-moment system. Numerical solution for the complete shock structure is obviously an immediate task.

In the DSMC study, the difficulty with the flux balances and the downstream boundary condition mentioned in §2.2 has very recently been resolved and the final realization of the quasi-1-D shock structure remains to be carried out.

3.5 Thermo-Chemical Nonequilibrium in Rarefied Hypersonic Flow

In terms of macroscopic variables, departure from translational equilibrium in a shock layer can affect the nonequilibrium thermo-chemistry in three ways. One is through the thermodynamic pressure or the density change due to translational nonequilibrium, and the second is through the translational temperature change. The third comes from a change in the rate constant and in the nature of the temperature dependence of the rate, which must depend, in principle, on the kinetics of the inelastic collision. Current treatment of such a problem in the DSMC frame work relies on the Borgnakke-Larsen ad hoc energy-transfer model of the inelastic collision [51] are no more reliable than the experimentally determined rates inferred in the continuum domain [19,20]. For a known/assumed excitation rate, the 13-moment based shock-layer theory developed in the present program allows one to treat the thermo-chemical nonequilibrium in a reduced NS system (in Doronitsyn or von Mises variable) with the rate altered by a factor of (P_{22}/p) where P_{22} may be identified with the pressure in the NS calculations, and p carries the influence of the translational nonequilibrium [11-15]. Solutions to this transformed thermal nonequilibrium NS problems can be used to *calibrate* new rates proposed for thermal nonequilibrium in rarefied hypersonic flow.

Simple relaxation type rate equations for the rotational and vibrational relaxation of diatomic gas similar to those used and cited in Refs. [52,20] should be considered in the reduced NS problem. An interesting study is provided by the flow around the shoulder of a blunt body, or on the expansion side of a plate or wing surface, where translational temperature freezing will have a significant influence on the freezing in rotational and vibrational energies (as well as chemistry).

Combustion involving detonation and deflagration waves in premixed fuel is an important aspect of hypersonic propulsion research. Definitive 2-D computational study has appeared recently only for the inviscid (Euler) problem [19,53]. The viscous and molecular transport processes are decisive factors in predicting ignition delay and deflagration front structure. Under the shock layer formalism, analytic or semi-analytic solution of the problem can be carried out as in the PI's earlier shock layer analysis [54]. The solution structure can be made more explicit by consideration of an Arrhenius rate with a high activation energy [55,56].

3.6 Hypersonic Boundary Layer Instability: Power-Law Shock and Görtler Instability

Recent development in hypersonic flow research [19] has brought out a number of generic instability problems, among which are the unstable inviscid instability at the boundary layer outer edge on slender bodies and on an aligned plate (even in the strong-interaction regime). Another instability is expected on a (curved) compression ramp in the form of a secondary instability associated the Görtler vorticity on the curved surface (cf. §2.3), which is believed to provide a mechanism of nonlinear instability preceding turbulence transition [19,57,58].

The instability analysis can be carried with basic technique not far from those in Refs. [59,60] and provide needed theoretical support to our time-accurate numerical analysis (§4.4).

4 Conclusion

Under AFOSR support (contract 1-0104), the depth and scope of a theory based on a thin-layer version of Grad's 13-moment equations, which allows correlation and prediction of flows in a hypersonic shock layer far from translational equilibrium with results of Navier-Stokes analyses, has been further developed to include detail studies of the distribution function, the numerical accuracy/adequacy, role of the transition similarity parameter P_{22}/p , and the applicability of the principle to studies comparing DSMC and more general NS based calculations.

Several versions of the thin-layer and time-dependent NS codes are programmed/implemented for the purpose of the comparison study, which promises an applicability range of the theory wider than anticipated. As examples of 3-D applications, the calculations from the PNS program establishes a concrete example of the numerical accuracy of the strip method (a property of the theory,) and leads to ways of generating a universal "bridging function" for flat-bottom lifting surface of a very wide planform class. The extensive computing effort has been spent on the time-accurate calculations of the flow-field evolutions upstream of a sharp trailing edge and of a deflected flap for a nonaligned flat plate. Several unique features are found to result from the extensive transonic flow region occurring in the viscous layer and the

extremely low temperature in some locality, which calls for an excessively small time step. The long computation time needed to carry out such a calculation represents an obstacle to be overcome for future application of NS codes in the $M_\infty = 20-25$ and $Kn = 10^{-1}-10$ ranges.

A glaring issue with the 13-moment based study has been its inability to provide a solution to the shock structure; this prevents a successful calculations for the entire flow field using shock-capturing technique and development of the shock-layer analysis to the next order. This is due to the failure of the distribution function stipulated, which fail to describe the persistent influence of the upstream-flow state in a hypersonic flow, as made evident by DSMC calculations and data inferred from experiment, as well as familiar Mott-Smith bi-modal analysis. The quasi-1-D shock structure analyses based on DSMC method and on a multimodal model have not yet proven fruitful, although the study with the multi-modal (moment) approach does succeed in resolving a major obstacle confounding Grad's original shock-structure analysis.

While much encouragement has been received in comparing the present theory (assuming $\gamma = 7/5$, $Pr = 0.72$) with DSMC calculations for model air. Similarly good agreement cannot be expected for a higher Mach number ($M_\infty > 27$) or for a lower altitude (< 80 km), owing to the inadequacy of the assumption of a fast rotation-translation energy transfer and frozen vibrational excitation and frozen air chemistry/ionization; introduction of appropriate assumptions modeling these nonequilibrium features for engineering applications remains to be implemented.

5 Publications and Documented Works Resulting from the Present Support

1. Cheng, H.K. 1991. *Proc. 4th Inter. Symp. Comp. Fluid Dynamics* Davis, Ca: 178-185
2. Cheng, H.K., Bao, Y., Lee, C.J., Wong, E.Y. 1992. *Proc. IUTAM Symp. Aerothermochemistry & Associated Hypersonic Flows*, Marseille, France (Sept. 1-4)
3. Cheng, H.K., Wong, E.Y., Hoover, L.N., Dogra, V.K. 1992. paper submitted to *AIAA J*; also *Proc. 1st Inter. Hypersonic Waverider Symp.* Univ. Maryland, Md, (Oct. 17-19 1990)
4. Cheng, H.K. 1993. *Annual Rev. Fluid Mech.*, 25: 455 -484
5. Cheng, H.K. 1993. Univ. So. Calif. Dept. Aerospace Eng. Report *USCAE 151*
6. Lee, C.J. 1993. "On the Unique Determination of Solutions to the Burnett Equations" (submitted to *AIAA J*; also Univ. So. Calif. Dept. Aerospace Eng. Report *USCAE-154*)
7. Yang, H.T. 1993. "Reduction of Grad 13-Moment Equations to Burnett Equations" (submitted to *J. Fluid Mechanics*; also Univ. So. Calif. Dept. Aerospace Eng. Report *USCAE-153*)
8. Shao, S., Cheng, H.K. 1993. "Maxwell Transfer Equations: Modification of Grad's System", I. Partial Differential Equations, Pitman Res. Notes Math. Series (ed. J. Wiener, J.K. Hale), Longman Sci. Tech. Essex. U.K.: 216-220

Papers, thesis, and reports in preparation are indicated in the Introduction and referred to as Refs. [18, 21, 22, 45] in the cited Reference below.

6 References

1. Bird, G.A. 1989. *Rarefied Gas Dynamics: Theoretical and Computational Techniques*, Progr. Astro. Aero. 118 (ed. E.P. Muntz et al), 221-226
2. Moss, J.N., Bird, G.A. 1985. *Thermal Design of Aeroassisted Orbital Transfer Progr. Astro. Aero. 96* (ed. H.F. Nelson): 113-139
3. Moss, J.N., Bird, G.A., Dogra, V.K. 1988. *AIAA paper 88-0081*
4. Chapman, S., Cowling, T.G. 1953. *The Mathematical Theory of Nonuniform Gases*, Cambridge Univ. Press
5. Vincenti, W. G., Kruger, C.H., Jr. 1965. *Introduction to Physical Gas Dynamics*, New York, Wiley
6. Kogan, M.N. 1969. *Rarefied Gas Dynamics* Moscow: Nauka (Transl. 1969 ed. L. Trilling, New York: Plenum)
7. Burnett, D. 1936. *Proc. London Math. Soc. Ser. 2* 40, no. 3: 382-435
8. Grad, H. 1949. *Comm. Pure Appl. Math.* 2, no. 4: 331-407
9. Cheng, H.K., Wong, E.Y. 1988. Univ. So. Calif. Dept. Aerospace Eng. Report USCAE 147
10. Cheng, H.K., Lee, C.J., Wong, E.Y., Yang, H.T. 1989. *AIAA paper 89-1663*
11. Cheng, H.K. 1989. *Proc. Inter. hypersonic Aerodynamics*, Univ. manchester, Manchester, England
12. Cheng, H.K., Wong, E.Y., Dogra, V.K. 1991. *AIAA paper 91-0783*
13. Cheng, H.K. 1991. *Proc. 4th Inter. Symp. Comp. Fluid Dynamics* Davis, Ca: 178-185
14. Cheng, H.K., Bao, Y., Lee, C.J., Wong, E.Y. 1992. *Proc. IUTAM Symp. Aerochemistry & Associated Hypersonic Flows*, Marseille, France (Sept. 1-4)
15. Cheng, H.K., Wong, E.Y., Hoover, L.N., Dogra, V.K. 1992. paper submitted to *AIAA J*; also *Proc. 1st Inter. Hypersonic Waverider Symp.* Univ. Maryland, Md, (Oct. 17-19 1990)
16. Lee, C.J. 1993. "On the Unique Determination of Solutions to the Burnett Equations" (submitted to *AIAA J*; also Univ. So. Calif. Dept. Aerospace Eng. Report USCAE-154)
17. Yang, H.T. 1993. "Reduction of Grad 13-Moment Equations to Burnett Equations" (submitted to *J. Fluid Mechanics*; also Univ. So. Calif. Dept. Aerospace Eng. Report USCAE-153)
18. Cheng, H.K. 1993. "On Extension of Continuum Models to Rarefied Gas Dynamics", paper to be presented at International Workshop on Advances in Modelling of Aerodynamic Flows, Miedzyzdroje, Poland (July 12-14)
19. Cheng, H.K. 1993. *Annual Rev. Fluid Mech.*, 25: 455-484
20. Cheng, H.K. 1993. Univ. So. Calif. Dept. Aerospace Eng. Report USCAE 151
21. Wong, E.Y. 1993. "Application and Validation of Grad's 13-Moment Theory to Hypersonic Shock-Layer Flows", Univ. So. Calif. Ph.D. Dissertation (August)
22. Wong, E.Y., Cheng, H.K., Dogra, V.K. 1993. "A Study of Rarefied Hypersonic Flows Using Grad's 13-Moment Equations" (paper in preparation)
23. Grad, H. 1952. *Comm. Pure Appl. Math.* 5, no. 3: 257-300

24. Shaaf, S.A., Chambré, P.L. 1958. *Fundamentals of Gas Dynamics* ed. H.W. Emmons. Sec. H, Princeton Univ. Press: 687-739
25. Rosenan, P., undated paper dedicated to the memory of Harold Grad (private communication)
26. Pham-Van-Diep, G.C., Erwin, D., Muntz, E.P. 1989. *Science* 245: 624-626; also *J. Fluid Mech.* 232: 403-413 (1991)
27. Cheng, H.K. 1963. *Cornell Aero. Lab. Report AF-1285-A-10*
28. Cheng, H.K. 1966. *Fundamental Phenomena in Hypersonic Flow*, ed. G.J. Hall, Cornell Univ. Press: 91-132
29. Mott-Smith, H.M. 1951. *Phys. Rev.* 82: 855-
30. Ikenberry, E., Truesdell, C. 1965. *J. Rat. Mech. Anal.* 5, no. 1,1-
31. Perminov, V.D., Fridlender, O.G. 1965. *Zhurnal Prikladnoi Mekhanike i Tekh. Fiziki*, 6, 114-116
32. Tammn I.E. 1965. *Trudy (Proc.) Lebedev Phys. Inst.*, 29: 231-241
33. Rudy, D.H., Thomas, J.L., Kumar, A., Gnoffo, P.A., Chakravathy, S.R. 1991. *AIAA J.* 29: 1108-1113
34. Vignerón, Y.C., Rakich, J.V., Tannehill, J.C. 1978. *AIAA paper 78-1337*
35. Brown, S.N., Cheng, H.K., Lee, C.J. 1990. *J. Fluid Mech.*, 220 : 309-537
36. Dogra, V.K., Moss, J.N., Price, J.M. 1989. *Rarefied Gas Dynamics* (ed. E.P. Muntz et. al.) *AIAA Conf. Series*, Acad. Press.
37. Dogra, V.K., Moss, J.N. 1989. *AIAA paper 89-1712*
38. Celenligil, M.C. Moss, J.N. 1991. *AIAA paper 91-1315*
39. Yashuhara, M., Nakamura, Y., Tanaka, J. 1989. *Rarefied Gas Dynamics* (ed. E.P. Muntz et. al.), 582-596
40. Zhong, X., MacCormack, R.W., Chapman, D.R. 1991b. *Proc. 4th. Inter. Symp. Comp. Fluid Dynamics*, Davis, Ca.
41. Zhong, X., MacCormack, R.W., Chapman, D.R. 1991a. *AIAA paper 91-0770*
42. MacCormack, R.W., Baldwin, B.S. 1975, *AIAA paper 75-1*
43. Hung, C.M., MacCormack, R.W. 1975. *AIAA paper 75-2*
44. Holden, M., Wieting, A.R., Moselle, J., Glass, C. 1988. *AIAA paper 88-0477*; also *NASP TN 1085* (1989)
45. Bao, Y., Lee, C.J. 1992. Univ. So. Calif. Sch. Eng. Dept. Aerospace Eng. Report *USCAE 152* (in preparation)
46. Bao, Y., Gursul, I., Lee, C.J. 1991. *Proc. 4th. Inter. Symp. Comp. Fluid Dynamics*, Univ. Calif. Davis, 1, 67-72
47. Moss, J.N., Price, J.M., Chun, C.H. 1991. *AIAA paper 91-1313*
48. Edney, B. 1968. *Aeron. Res. Inst. Sweden, Stockholm, Rept. 115*; also *AIAA J.* 6, 15-21
49. Liepman, H.W., Roshko, A. 1957. *Elements of Gas Dynamics*, Wiley
50. Emanuel, G. 1986. *Gasdynamics: Theory and Applications*, 387-397; 425
51. Borgnakke, C., Larsen, P.S. 1975. *J. Computational Physics* 18: 405-420
52. Lumpkin, F.E., Chapman, D.R. 1991. *AIAA paper 91-0771*, also see Lumpkin, F.E., Chapman, D.R., Park, C. 1989. *AIAA paper 89-1737*

53. Wilson, G.J., MacCormack, R.W. 1992. *AIAA J.* 30, 1008-1015
54. Cheng, H.K. 1961. *Proc. Heat Transfer and Fluid Mech. Inst.*, ed. R.C. Bender et al. Stanford Univ. Press: 161-175
55. Cheng, H.K., Lee, R.S. 1968. *AIAA J.*, 6, 823-838
56. Buckmaster, J., Ludford, G. 1988 *Mathematical Modeling in Combustion Science*, Springer Verlag
57. Spall, R.E., Malik, M.R. 1989. *Phys. Fluid A*, 1: 1822-1835
58. Malik, M.R., Zang, T., Bushnell, D. 1990. *AIAA paper 90-5232*
59. Smith, F.T. 1989. *J. Fluid Mech.* 198: 127-153
60. Smith, F.T., Brown, S.N. 1990. *J. Fluid Mech.* 219: 499-518
61. Shao, S., Cheng, H.K. 1993. "Maxwell Transfer Equations: Modification of Grad's System", I. Partial Differential Equations, Pitman Res. Notes Math. Series (ed. J. Wiener, J.K. Hale), Longman Sci. Tech. Essex. U.K.: 216-220